Exfoliation and Characterization of Two Dimensional TiB$_2$ Nanosheets

By

Marghoob Ahmed

(Registration No: 00000362369)

Department of Materials Engineering

School of Chemical and Materials Engineering

National University of Sciences & Technology (NUST)

Islamabad, Pakistan

(2024)

Exfoliation and Characterization of Two Dimensional TiB$_2$ Nanosheets

By

Marghoob Ahmed

(Registration No: 00000362369)

A thesis submitted to the National University of Sciences and Technology, Islamabad,

in partial fulfillment of the requirements for the degree of

Master of Science in
Nanoscience and Engineering

Supervisor: Dr. Sofia Javed

School of Chemical and Materials Engineering

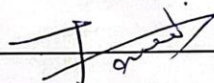National University of Sciences & Technology (NUST)

Islamabad, Pakistan

(2024)

THESIS ACCEPTANCE CERTIFICATE

THESIS ACCEPTANCE CERTIFICATE

Certified that final copy of MS thesis written by Mr **Marghoob Ahmed** (Registration No 00000362369), of School of Chemical & Materials Engineering (SCME) has been vetted by undersigned, found complete in all respects as per NUST Statues/Regulations, is free of plagiarism, errors, and mistakes and is accepted as partial fulfillment for award of MS degree. It is further certified that necessary amendments as pointed out by GEC members of the scholar have also been incorporated in the said thesis.

Signature: _____

Name of Supervisor: **Dr Sofia Javed**_____

Date: ____13-2-24_____

Signature (HOD): _____

Date: ____13/2/27_____

Signature (Dean/Principal): _____

Date: ____14.2. 2024_____

TH - 1

National University of Sciences & Technology (NUST)
MASTER'S THESIS WORK

Formulation of Guidance and Examination Committee (GEC)

Name: Marghoob Ahmed

NUST Reg No: 00000362369

Department: Department of Materials Engineering

Specialization: Master of Science in Nanoscience & Engineering

Credit Hour Completed: 24.0

CGPA: 4.0

Course Work Completed

S/No:	Code:	Title:	Core/Elective:	CH:	Grade:
1.	NSE-813	Essentials of Nanoscience and Engineering	Compulsory	3.0	A
2.	MSE-854	Characterization Of Materials	Compulsory	3.0	A
3.	RM-898	Research Methodology	Additional	2.0	Q
4.	NSE-845	Nanolithography And Device Fabrication	Elective	3.0	A
5.	MSE-856	Nano Material and Processing	Compulsory	3.0	A
6.	MSE-862	Electronic And Magnetic Materials	Elective	3.0	A
7.	MSE-952	Materials For Biomedical Applications	Elective	3.0	A
8.	MSE-954A	Advanced Characterization Of Materials	Elective	3.0	A
9.	NSE-843	Nano Technology And Photovoltaics	Elective	3.0	A
10.	ESE-904	Advanced Energy Materials: Synthesis & Characterization	Additional	3.0	A

Date 04 - Nov - 2022

Student's Signature

Thesis Committee

Name: Sofia Javed (Supervisor)
Department: Department of Materials Engineering

Signature

Name: Iftikhar Hussain Gul (Internal)
Department: Department of Materials Engineering

Signature

Name: Sarah Farrukh (Internal)
Department: Department of Chemical Engineering

Signature

Date: 04 - Nov - 2022

Signature of Head of Department:

APPROVAL

Date: 04 - Nov - 2022

Signature of Dean/Principal:

School of Chemical & Materials Engineering (SCME) (SCME) H-12 Campus.

TH – 4

National University of Sciences &Technology (NUST)

FORM TH-4

MASTER'S THESIS WORK

We hereby recommend that the dissertation prepared under our supervision by

Regn No & Name: <u>00000362369 Marghoob Ahmed</u>

Title: <u>Exfoliation and Characterization of Two Dimensional TiB$_2$ Nanosheets.</u>

Presented on: <u>01 Feb 2024</u>   at: <u>1400 hrs in SCME Seminar Hall</u>

Be accepted in partial fulfillment of the requirements for the award of Masters of Science degree in <u>Nanoscience & Engineering.</u>

Guidance & Examination Committee Members

Name: <u>Dr Sarah Farrukh</u>   Signature: _____

Name: <u>Dr Iftikhar Hussain Gul</u>   Signature: _____

Supervisor's Name: <u>Dr Sofia Javed</u>   Signature: _____

                    Dated: <u>12 - 2 - 24</u>

_____   _____

Head of Department   **Dean/Principal**

Date ___12/2/24___   Date ___12.2.2024___

School of Chemical &Materials Engineering (SCME)

AUTHOR'S DECLARATION

I Marghoob Ahmed hereby state that my MS thesis titled "Exfoliation and Characterization of Two Dimensional TiB$_2$ Nanosheets" is my own work and has not been submitted previously by me for taking any degree from National University of Sciences and Technology, Islamabad or anywhere else in the country/ world.

At any time if my statement is found to be incorrect even after I graduate, the university has the right to withdraw my MS degree.

Name of Student: Marghoob Ahmed

Date: 19 February 2024

PLAGIARISM UNDERTAKING

I solemnly declare that research work presented in the thesis titled "Exfoliation and Characterization of Two Dimensional TiB_2 Nanosheets" is solely my research work with no significant contribution from any other person. Small contribution/ help wherever taken has been duly acknowledged and that complete thesis has been written by me.

I understand the zero-tolerance policy of the HEC and National University of Sciences and Technology (NUST), Islamabad towards plagiarism. Therefore, I as an author of the above titled thesis declare that no portion of my thesis has been plagiarized and any material used as reference is properly referred/cited.

I undertake that if I am found guilty of any formal plagiarism in the above titled thesis even after award of MS degree, the University reserves the rights to withdraw/revoke my MS degree and that HEC and NUST, Islamabad has the right to publish my name on the HEC/University website on which names of students are placed who submitted plagiarized thesis.

Student Signature: _____

Name: Marghoob Ahmed

DEDICATION

"To my Grand Father, who is no longer with me to witness me complete my work. May I have the same unwavering dedication to my field in science that you had in me."

ACKNOWLEDGEMENTS

TABLE OF CONTENTS

LIST OF TABLES

LIST OF FIGURES

LIST OF SYMBOLS, ABBREVIATIONS AND ACRONYMS

Ultrasonication	US
Liquid Phase Exfoliation	LPE
Energy Density	ED
Inertial Cavitation Dosage	ICD
Cavitation Field	CF
Cavitation Intensity	CI
Cavitation Zone	CZ
Cavitation Bubbles	CB
Acoustic Power	AP
Bulk Titanium Diboride	BTB
Two Dimensional Nanomaterials	2D
Two Dimension TiB_2 Nanosheets	2D TiB_2
Few Layered 2D TiB_2	FLTB
N-methyl-2-pyrrolidone	NMP
De-Ionized Water	DIW

Transition Metal Diborides   TMB

Bulk Form   BF

Nanomaterials   NM

ABSTRACT

The substance known as 2D TiB$_2$ is a newly discovered two-dimensional material. Liquid Phase Exfoliation (LPE) is widely recognized for its efficacy in exfoliating 2D TiB$_2$. This method is particularly suitable for meeting the requirements of large-scale industrial production. However, most of the currently available liquid-phase exfoliation (LPE) procedures require the utilization of harmful and expensive solvents for the chemical exfoliation of the two-dimensional (2D) sheets prior to their mechanical (ultrasonic) dispersion. In the present study, a comparison was conducted to assess the impacts of two dispersive mediums, namely NMP and DI Water. Subsequently, we conducted an analysis on the effects of significant ultrasonic (US) LPE parameters, namely Input Power and US Treatment Time, to control the efficient production and enhance the quality of few layered 2D TiB$_2$ sheets within a limited duration, particularly in a pristine aquatic setting. The findings of our study indicate that the liquid phase exfoliation (LPE) process in N-methyl-2-pyrrolidone (NMP) consists of three distinct steps, whereby contaminants are present in the exfoliated sheets. This characteristic renders the procedure time-consuming and expensive. In contrast, the liquid phase exfoliation (LPE) technique employed in this study was shown to be a one-step procedure that yielded defect-free, highly pure, and systematically exfoliated sheets. Consequently, this approach is considered as environmentally friendly, devoid of impurities, and cost-effective. The key factors that influence the reduction of layer thickness, lateral dimensions, and manufacturing yield of 2D TiB$_2$ include the input power of an ultrasonic (US) source, a higher intensity of acoustic cavitation, an optimal duration of US treatment, and a uniform distribution of cavitation events achieved by employing a suitably sized sonotrode within the sonicated volume. This work offers a means to enhance the LPE methodology as a financially feasible, environmentally friendly, and readily scalable manufacturing approach for the large-scale commercial production of 2D TiB$_2$. These 2D TiB$_2$ sheets may be applied in several domains such as energy storage, water splitting, and catalytic processes.

GRAPHICAL ABSTRACT
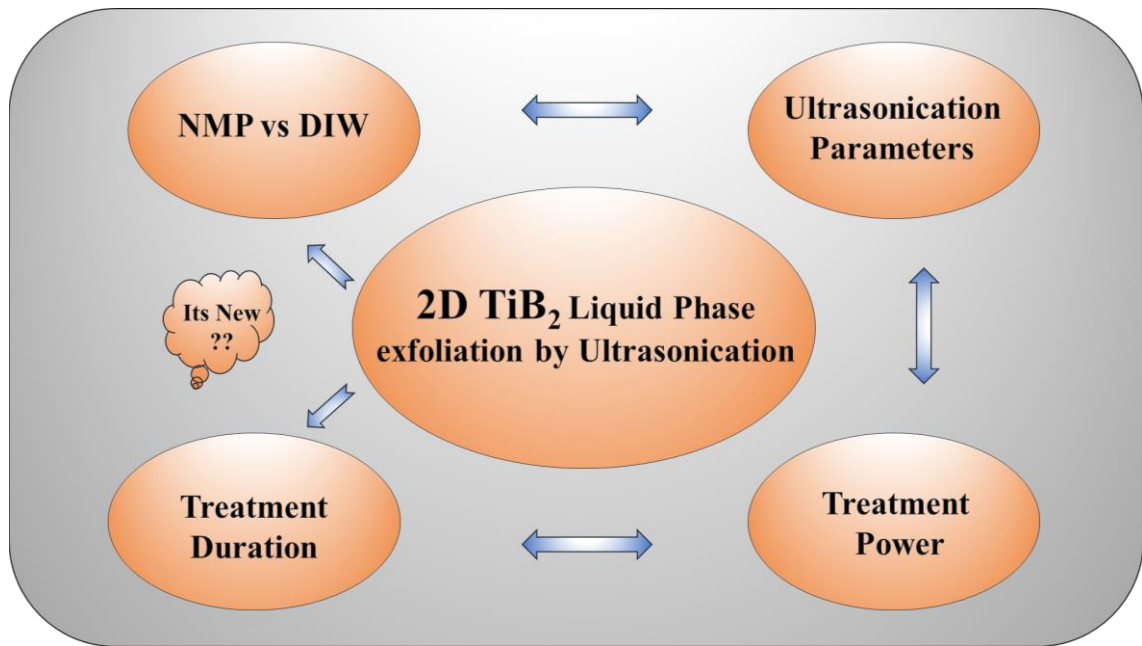
CHAPTER 1:   INTRODUCTION

1.1   Background

Nanomaterials can be defined as materials with dimensions ranging from 1 to 100 nanometer in one, two, or all three dimensions [1]. Examples of such materials include quantum dots, nanofibers, nanowires, and nanoplates, which exhibit particle aggregation or agglomeration within the size range of 1 to 100 nm [2]. The developing area of Nanotechnology is involved in the synthesis of nanomaterials with distinct features by the manipulation of their size, shape, or crystallinity [3].

Nanomaterials are increasingly being utilized across several domains, including but not limited to medicine, environmental science, and industry, owing to their remarkable characteristics [3-5]. They are often employed in a wide range of contemporary commercial sectors [6, 7], serving as fillers, filtration agents, electronic components, semiconductors, and in biomedical applications such as biosensors, cosmetics, biochips, nanomedicines, and bioelectronics [8, 9]. The synthesis of materials with dimensions below 100nm is a multidisciplinary endeavor that incorporates several fields within the realm of nanotechnology [10, 11].

The physiochemical characteristics of Two Dimensional (2D) nanomaterials are remarkable because of their freestanding sheets and their high aspect ratio, where the lateral size is larger than 100nm and the thickness is less than 100nm [3, 12, 13]. These materials possess a thickness at the atomic scale and have remarkable characteristics such as ultrahigh carrier mobilities, a very large surface area, quantum hall effects, transparency, and outstanding applications [14].

Two-dimensional (2D) materials exhibit enhanced thermal conductivity, matchless strength, amazing optical properties, great flexibility, remarkable stability, and extraordinary carrier transport capabilities [3, 15]. These materials exhibit a range of bandgaps, including both zero and large bandgaps [8-11, 16], making them suitable for

many applications such as energy storage, sensing, electronics, photodetectors, drug delivery, and more [4, 5].

Two-dimensional (2D) nanomaterials are classified as crystalline materials that possess structures resembling freestanding sheets [6, 7, 14, 17-19]. The materials in question possess a singular layer or a limited number of atomic layers, with lateral dimensions ranging from over 100 nm to a few micrometers. In general, the thickness of these entities is often below 50nm [20].

The layers of atoms exhibit a significant degree of interaction, resulting in the formation of several single or multi-layered 2D structures [21] that possess distinct physicochemical properties [22]. The seminal year for 2D materials is 2004, when Novoselov et al. [23] employed the micromechanical cleavage approach, utilizing Scotch tape to exfoliate graphite and successfully generate graphene [13].

1.1.1   *Bulk 2D Materials*

In the context of bulk materials, the antecedents of 2D materials refer to solids that exhibit robust covalent or ionic bonding between atoms in a layer, whereas the interlayer attachment is facilitated by comparatively weaker forces [24].

Therefore, by the application of shear stress or the introduction of intercalating chemicals, these layers can expand in an out-of-plane manner or slide in an in-plane direction during the process of exfoliation, resulting in the formation of a few-layer or monolayer of two-dimensional flakes [25].

1.2   Transition Metal Diborides

Transition Metal diborides are a type of compound that exhibits a ceramic character [26, 27]. Metals M are classified under Groups II, IV-B, and V-B, exemplified by elements such as Titanium (Ti), Zirconium (Zr), Magnesium (Mg), Chromium (Cr), among others [28]. Bulk metal borides have several applications, including their usage as catalysts, semiconductors, conductive ceramics, and hard magnets [29, 30]. The researchers prioritize the investigation of many significant features [27, 31], including

luminescence, ultra-hardness, field-emission, conduction, thermoelectricity, and magnetism [32-34].

The subject of inquiry pertains to their exceptional characteristics, which encompass heightened hardness, elevated melting point and thermal conductivity, resistance to wear, augmented strength, and chemical stability. Transition metal diborides are a class of materials that possess a combination of metallic and ceramic characteristics, hence placing them within the classification of ultrahigh temperature ceramics [35-37].

1.2.1 Bulk 2D Materials

Refractory borides, namely TaB_2, TiB_2, ZrB_2, and HfB_2, exhibit great potential as suitable options for various ultra-high temperature applications such as cutting tools, rocket nozzles, electrodes, wear resistant parts, and armor. This is primarily due to their remarkable melting temperatures, which can reach approximately 4000 °C, as well as their exceptional chemical and thermomechanical properties [38-42].

Due to their exceptional characteristics when exposed to high temperatures, these materials possess the potential to be utilized in the production of various components such as nose tips, hot structural components for hypersonic vehicles, scramjet engines, and microelectronics [27, 43-46].

1.3 Titanium Diboride

Titanium diboride is a notable member within the category of transition metal diborides due to its exceptional electrical conductivity, measured at 22 x 10^6 $\Omega^{-1}cm^{-1}$ [47-49]. Additionally, it possesses a high melting point of 3225 °C, an increased hardness range of approximately 25-35 GPa, a relatively low density of 4.5 g/cm^3, and exhibits chemical stability at elevated temperatures. Furthermore, it demonstrates superior thermal conductivity, measuring at 96 W/mK [47-49].

These characteristics render TiB_2 a promising candidate for many applications such as cutting tools, weaponry, wear and erosion resistance, crucibles, high-temperature

electrodes, microelectronics, mechanical components, and high-temperature structural purposes [49-52].

1.3.1 2D Transition Metal Diborides

The existence of various 2D metal borides have been predicted and some of which are made through experimentation. Alternative boron and titanium sheets are present in layered (Titanium Diborides) TiB_2 inorganic material [53-56]. The solvent dispersion of 2D nanosheets can be prepared by exfoliation of this bulk TiB_2 in liquid medium having high ratio of boron to titanium, which can be used for applications having boron-based 2D nanosheets [57, 58].

Due to small dimensions, 2D Titanium Diborides will have different optical and chemical properties, unique mechanical strength, and other properties than the bulk material which must be investigated [55]. These properties can be utilized in optical, electronics, magnetic, energy conversion and storages applications [31, 53].

1.4 Synthesis of 2D Materials

Top-down methodologies encompass several techniques such as mechanical compression, nanolithography, exfoliation, micromechanical cleavage, chemical vapor deposition, ball milling, and Hummer's method [3, 12, 59-61]. The prevalent techniques employed for the fabrication of two-dimensional (2D) materials encompass chemical vapor deposition (CVD), scotch deposition, physical vapor deposition, and micromechanical cleavage [3, 13, 23, 62].

The micromechanical fracturing of bulk-layered crystalline formations can be achieved with the introduction of one or a few layers of 2D nanomaterials [63, 64]. Prior studies have indicated that the approaches now in use are associated with substantial production expenses and have little potential for expansion. The process of ball milling has the capability to generate nanosheets on a massive scale [59, 65]; nevertheless, it also leads to the introduction of flaws in these two-dimensional structures [66-68].

1.4.1 Liquid Phase Exfoliation

The manufacture of two-dimensional (2D) nanosheets is predominantly achieved using the widely used technique of exfoliation [60]. The mechanical exfoliation technique, often known as the standard approach for generating 2D nanosheets, has restricted practicality when considering its applicability on a large-scale commercial level [69]. The liquid-phase exfoliation (LPE) technology has been shown to be very suitable for large-scale manufacture and has thus become the main method for producing commercially available 2D materials [66, 68, 70].

Nevertheless, it is important to acknowledge that the liquid-phase exfoliation (LPE) technique, which operates in a top-down manner, has a notably poor efficiency in terms of yield [71] and necessitates the elimination of a considerable amount of unexfoliated [63] bulk material [63, 72, 73]. However, the technique's remarkable scalability and cost-effectiveness make it suitable for the high-volume manufacturing of two-dimensional (2D) materials [72, 73]. Moreover, the quality of these materials surpasses that of synthesized 2D materials produced using ball milling or chemical routes, exhibiting fewer or insignificant flaws [66-68].

1.4.2 Steps of Conventional Liquid Phase Exfoliation

LPE offers the capacity to manufacture 2D sheets with precise thickness control, exhibiting a range of flake shapes and sizes, various numbers, and types of defects, as well as well-defined surfaces and edges [71, 74]. This facilitates the satisfaction of various demands for developing applications, such as filters, biomarkers, ink, epoxy composites, and other related areas [75-80].

Nevertheless, the current LPE approaches exhibit significant limitations, as discussed in prior research [64, 71]. The methods commonly employed in this context typically encompass three approaches [64, 71, 81].

- Firstly, the use of solvents or surfactants that are costly, hazardous, and environmentally harmful is employed for chemical treatment processing. This process aims to enhance the interlayer spacing of bulk 2D material.

- Secondly, external forces such as shearing or ultrasonication are applied to aid in the exfoliation and dispersion of 2D flakes within a solution.

- Lastly, it is often necessary to purify 2D sheets to eliminate any remaining chemicals.

The utilization of ecologically sustainable and non-toxic dispersants to produce two-dimensional sheets is emphasized in a new investigation on liquid phase exfoliation (LPE) [71].
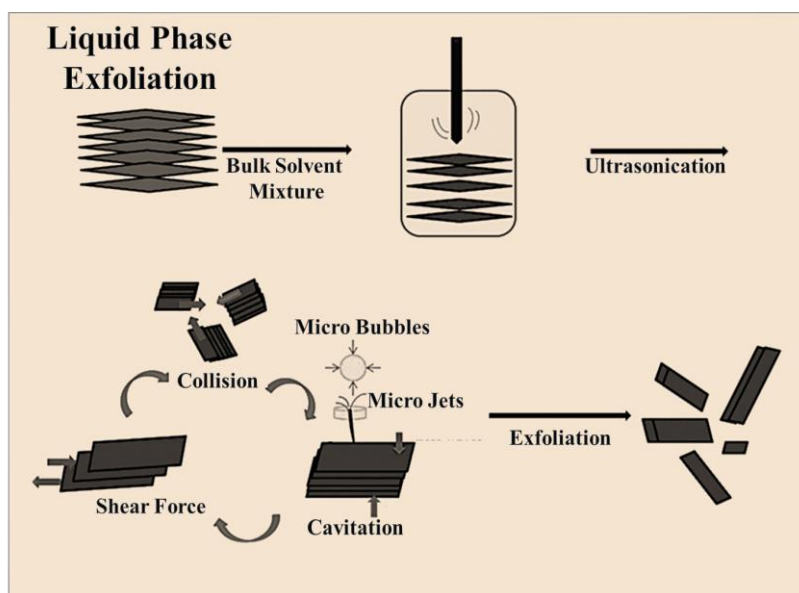
Figure 1.1:*: Liquid Phase Exfoliation*

1.4.3 Novel Dispersant for Liquid Phase Exfoliation

Water is an optimal and attractive choice for the dispersive medium, particularly due to the hydrophilic properties of many 2D materials [82]. This characteristic makes water a favorable and cost-effective medium for dispersion while also being environmentally friendly [83, 84].

Several studies have been conducted on water-based liquid phase exfoliation (LPE) that have used surfactants, polymer stabilizers, or other specialized chemicals as

exfoliation agents [85-89]. These components are deemed essential for achieving the dispersion of 2D flakes in water [89, 90].

Based on the available knowledge, there exists a lack of reported cases when the process of titanium diboride (TiB_2) exfoliation through ultrasonication has been carried out solely employing water as the medium [26, 57, 91-93]. Previous research on other 2D material has shown that the treatment modality required a significant duration [94].

According to several sources, it has been proposed that a supplementary exfoliation procedure including the utilization of N-methyl-2-pyrrolidone (NMP), dimethylformamide (DMF), or isopropyl alcohol (IPA) as a pre-treatment is necessary [58, 91, 93].

Typically, these steps are essential for initiating the processing of the TiB_2 source. In these approaches, the primary function of ultrasonic (US) processing is to maintain the dispersion of a few layer flakes inside the solution [95, 96].

1.5   Ultrasonic Parameters

The manipulation of sonication power and sonication duration serves as crucial factors in regulating the lateral dimension, layer thickness, and concentration of the two-dimensional dispersion [97]. The application of ultrasonic treatment on the bulk material results in a reduction in layer thickness through the cavitation process, while also facilitating the creation of a stable dispersion of 2D material [98].

The effectiveness of sonication treatment is primarily determined by two key parameters: sonication strength and sonication time [99-101]. The stability of nanomaterial dispersions is also influenced by the power and duration of ultrasonication. The dispersions exhibit maximum stability when they are subjected to optimal power and duration [100, 102].

The several process elements that need to be considered include the source of bulk TiB_2, the concentration of the solution being tested, the presence of surfactants, the form

of the vessel, the temperature (T), the size of the probe, and the shape of the ultrasonic (US) reactor [101, 103].

1.6   Parametric Investigation of Liquid Phase Exfoliation

The preparation of a solvent dispersion of two-dimensional Titanium Diboride nanosheets (2D TiB_2) involves the exfoliation of Bulk Titanium Diboride (BTB) in water having a boron to titanium ratio that is rather high [58]. Based on current understanding, there exists a lack of research that has explored the utilization of water as the only medium for conducting ultrasonication-induced Transition metals diborides (TMB) exfoliation [26, 57, 91-93].

Several studies done on the US liquid phase exfoliation (LPE) of two-dimensional (2D) materials suffer from a lack of thorough understanding of the fundamental mechanisms that dictate the exfoliation process [104].

This study focuses on the potential problems arising from the widespread use of solvents or surfactants, the application of the US-assisted LPE technique in pure DI water as a one-step process, and the influence of various key parameters such as input power, time, and setup configuration on the LPE process of 2D TiB_2.

The technology utilized in the present work effectively showcases the capacity to produce a limited number of high-quality, multi-layered 2D TiB_2 sheets using just deionized water.

CHAPTER 2: LITERATURE REVIEW

2.1   2D Materials

Prominent examples of two-dimensional (2D) nanomaterials encompass Graphene, h-BN (Hexagonal Boron Nitride), GO (Graphene Oxide), rGO (reduced Graphene Oxide), LDHs (Layered double hydroxide), TMDs (transition metals dichalcogenide), g-C_3N_4 (graphitic-carbon nitrides), layered metal oxides, MXenes, noble metals, COFs (Covalent organic framework), MOFs (metal organic framework), polymers, BP (Black Phosphorus), silicene, antimonene, inorganic perovskites, and organic−inorganic hybrid perovskites [12, 105, 106].
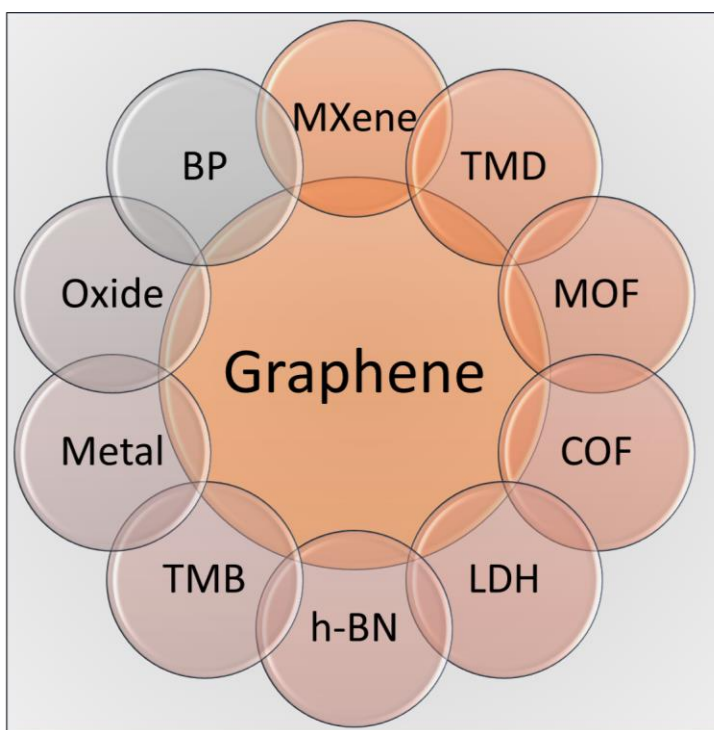
Figure 2.1: Examples of 2D Materials previously exfoliation

Two-dimensional (2D) nanomaterials possess several benefits [107]. The confinement of electrons in two dimensions gives rise to remarkable electrical characteristics and optical transparency, presenting a fresh avenue for exploring condensed matter physics and potential applications in optoelectronics [107].

The remarkable mechanical strength and flexibility exhibited by 2D nanomaterials can be attributed to their atomic thinness and the presence of robust covalent bonding inside the plane [10, 11]. These unique properties make them highly suitable for incorporation into advanced gadgets of the future [10, 11].

The 2D nanomaterial's ultrahigh specific surface area offers significant advantages for surface-related devices such as catalysis and supercapacitors [8, 9]. The synthesis of a few layers of 2D nanomaterials with a solution-based approach yields sheets of exceptional quality, which may be effectively used in various practical applications such as supercapacitors or solar cells [6, 7].

Two-dimensional (2D) nanomaterials are materials that have surfaces on both sides, making them suitable for surface engineering, modification, or doping processes [14].

2.2   Bottom-up Synthesis of 2D Materials

Multiple methods exist to produce two-dimensional nanomaterials. In bottom-up methodologies, the synthesis of nanomaterials involves the initial assembly of individual atoms or molecules to form larger structures [108-110].

Bottom-up techniques in materials synthesis encompass a range of methods, such as organic ligand aided synthesis, solvothermal synthesis, hydrothermal synthesis, polyol synthesis, templated based synthesis, photochemical synthesis, biological synthesis, wet chemical synthesis, and seeded synthesis [108-110].

The compatibility of the substrate with 2D materials has significant importance in these methodologies because of their reliance on the growing surface.
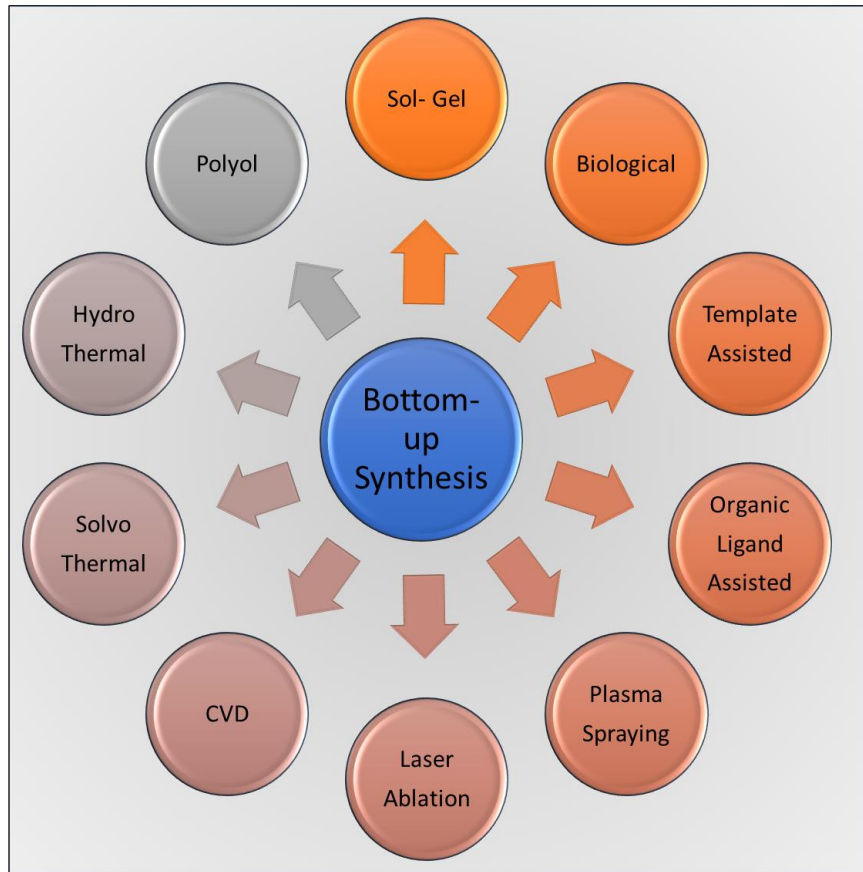
Figure 2.2: Bottom-up Synthesis methods of 2D Materials.

2.2.1   2D Materials by Sol-Gel

The sol-gel synthesis is the most famous method in which Sol, which is chemical solution is converted into Gel which is interlinked structure of particles to produce the 2D nanomaterials. Metal oxides and Chlorides are usually the starting precursors.

The precursors are dissolved into the solvent and gel is formed by sonication or stirring. Chemical vapor deposition is used to produce extremely pure and controlled thickness 2D nanomaterials which is done by depositing a controlled layer of gaseous precursors on any substrate by the chemical reaction at room temperature [3, 12, 13].

11

2.3   Top-Down Synthesis of 2D Materials

Top-down methodologies encompass many techniques such as mechanical compression, nanolithography, exfoliation, micromechanical cleavage, Chemical vapor deposition, and Hummer's method [3, 13, 23, 62].
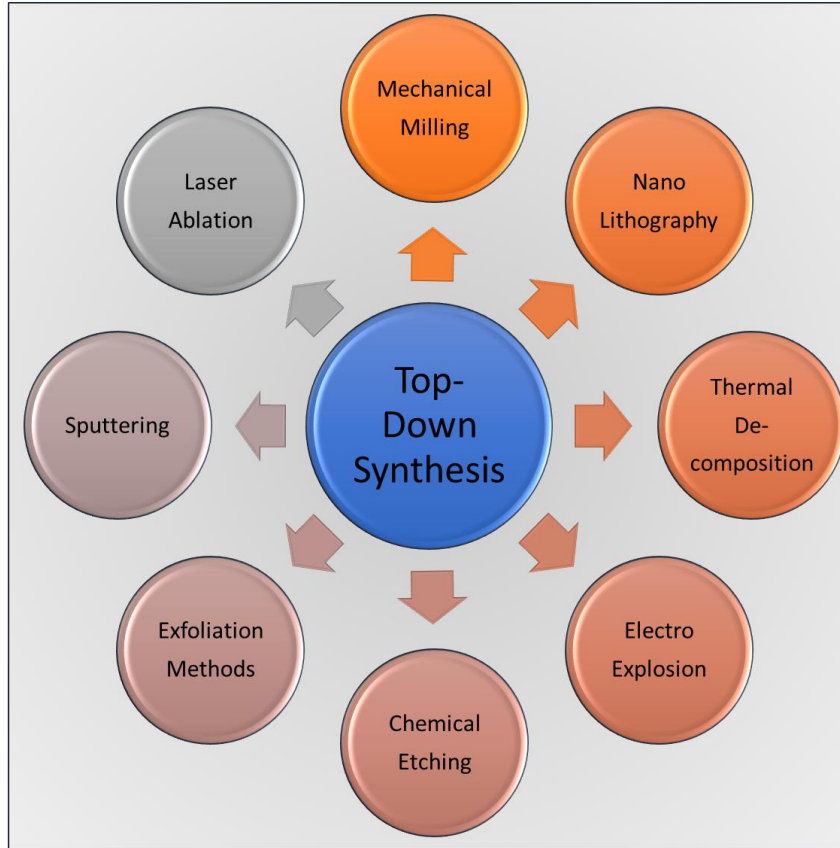
Figure 2.3: Top-Down Synthesis methods of 2D Materials.

Top-down techniques involve the initial utilization of bulk materials, which are then fragmented to provide 2D nanomaterials. The production of 2D nanomaterials involves the utilization of mechanical milling for grinding purposes, followed by a post-annealing process. Lithography is a viable method to produce patterned two-dimensional materials with diverse architectures. A laser beam is employed to concentrate a plasma plane within a solution after its interaction with a metal [3, 13, 23, 62].

Sputtering is a viable method to produce thin 2D nanomaterials characterized by a monolayer or a limited number of layers. Thermal decomposition induces the dissociation

of chemical bonds within the compounds, resulting in the formation of two-dimensional (2D) materials [111, 112].

2.3.1   Common Methods of Synthesis of 2D Materials

The most often employed techniques for synthesizing 2D materials are chemical vapor deposition (CVD), scotch deposition, physical vapor deposition (PVD), and micromechanical cleavage. The conversion of bulk layered crystalline formations into single or few-layered 2D nanomaterials is achieved by the process of micromechanical cleavage. Various exfoliation processes can be employed for the purpose of producing and regulating the morphology and dimensions of exfoliated sheets [66, 113, 114].

The manufacturing of two-dimensional (2D) nanosheets commonly uses exfoliation as the prevailing technique. Various exfoliation strategies encompass ion exchange-assisted or ion intercalation-assisted methods, selective etching-assisted approaches, oxidation-assisted procedures, mechanical force-assisted techniques, sonication or shear force-assisted methodologies, and electrochemical exfoliation [3, 12, 59-61].

2.3.2   Problems with the Common Methods

A persistent obstacle within the realm of 2D material synthesis pertains to the attainment of a harmonious equilibrium among several aspects, including but not limited to quality, affordability, scalability, purity, and yield of the 2D flakes. There exist many methodologies to produce two-dimensional nanomaterials [65, 115].

Bottom-up methods in materials synthesis encompass a range of techniques, such as organic ligand-assisted synthesis, solvothermal synthesis, hydrothermal synthesis, polyol synthesis, template-based synthesis, photochemical synthesis, biological synthesis, wet chemical synthesis, and seeded synthesis. The reliance of growth surfaces makes substrate compatibility crucial in the context of these approaches involving 2D materials. Moreover, these techniques have the potential to undermine the integrity and homogeneity of the fabricated two-dimensional sheets. The utilization of chemical pathways facilitates the production of the substance on a significant scale, resulting in a substantial output while

maintaining a comparatively economical expense. Nevertheless, the existence of impurities compromises the quality of the final 2D sheets [116-118].

From an industrial standpoint, it is important to investigate a wide range of 2D flakes to meet the varying needs of different applications. For example, the integration of thermally expanded 2D materials into epoxy composites has been demonstrated to improve their thermal, fire, and heat resistance properties, as well as their thermal conductivity. These 2D materials are synthesized through a multistep process that involves liquid phase exfoliation aided by ultrasonication. Small-sized flakes of few-layer sheets with a well-developed surface have been employed in several applications, including inkjet circuits, printed medical sensors, biosensors, and gas vapor sensors [76, 80, 119-122].

A noteworthy new discovery concerns the possible application of micrometer-sized 2D sheets with a limited number of layers in filtration processes, namely in the conversion of saltwater into drinkable water [123].

2.4   Liquid Phase Exfoliation

Micromechanical cleavage enables the exfoliation of single or few layer 2D materials using mechanical stress on bulk layered materials. The process of exfoliating ultrathin 2D nanoflakes from bulk stacked material involves distributing the components in a liquid media and applying suitable mechanical force. Various mechanical pressures can be utilized to facilitate the exfoliation of bulk layered materials, enabling their large-scale manufacture with high yields [63, 64].

The forces in question might manifest as either shear forces or because of sonication in the liquid phase. Sonication is the use of an external force to disrupt the relatively weak intermolecular van der Waals interactions that exist between layers of materials. Sonication is a process that generates shear forces and induces cavitation, which refers to the formation and subsequent collapse of microscopic bubbles, to facilitate the exfoliation of the material [3, 124, 125].

The process of liquid phase exfoliation using sonication is widely employed and considered to be the most straightforward approach to produce two-dimensional

nanosheets from bulk materials. The bulk layered materials are dispersed in a suitable solvent, such as Deionized Water (DI), N-methyl-pyrrolidone (NMP), or Isopropyl Alcohol (PVA), prior to undergoing sonication for a specified period. Centrifugation is employed to get a homogeneous dispersion of pure two-dimensional nanosheets after the process of sonication [126, 127].

2.4.1 Exfoliation Process

Cavitation and bubble formation occur within the liquid medium. Upon the collapse of these bubbles, shock waves and microjets are generated, which propagate through the bulk layered material dispersed in the solvent. This process results in the creation of a localized hotspot characterized by exceedingly high temperature and pressure, thereby yielding a substantial amount of energy [63, 64].

Consequently, this energy facilitates the exfoliation of the bulk material into ultrathin 2D nanosheets. To accomplish successful exfoliation, it is crucial for the energy of the exfoliation to be compatible with that of the bulk layered material. The proposed method exhibits characteristics such as cost-effectiveness, scalability, and high productivity, making it a viable approach for synthesizing 2D nanomaterials on a wide scale. Various solvents can be employed for the purpose of liquid phase exfoliation using sonication, to achieve the exfoliation of bulk layered materials such as TiB_2, ZrB_2, etc. [124, 128].

Previous findings suggested that the selection of a suitable solvent, characterized by a high degree of surface tension compatibility with the layered material, can effectively reduce the energy required for exfoliation. The prevention of aggregation and restacking, as well as the achievement of a stable dispersion of 2D nanosheets, were considered as the crucial functions of the solvent. Water may be employed as a means of exfoliating bulk layered materials through the process of sonication. This results in the production of a stable dispersion, which can be attributed to the inherent wettability of the nanosheets. Efficient exfoliation by sonication may be obtained via liquid phase exfoliation when there is a favorable match between the forces present in bulk layered material and energy of the ultrasonic source [81].

15

Various additives, including surfactants and polymers, can be employed in aqueous media to enhance exfoliation by modulating surface tension. The regulation of lateral dimension, layer thickness, and concentration of the 2D dispersion is dependent on several important parameters, including sonication power, vessel form, sonication time, solvent, sonication temperature, and additives [129, 130].

Several challenges remain to be addressed in liquid phase exfoliation. These include the limited yield of single layer exfoliation dispersion, the small lateral dimensions resulting from sonication-induced breakage of in-plane bonds, the presence of undesirable residual substances on the surface, and the potential introduction of defects during the exfoliation process [115, 131, 132].

2.5   Transition Metal Diborides

Metal diborides constitute a substantial assemblage of no less than 30 distinct components within the periodic table. Most of these materials have a hexagonal structure of the AlB_2 type, characterized by boron layers that closely resemble graphitic layers [28, 133, 134].

The covalent interaction between boron atoms in 3D metal diboride complexes facilitates their structural integrity. The presence of boron layers in these diborides contributes to their elevated electrical conductivity. The configuration of boron atoms has a significant impact on both the chemical and physical characteristics. The scientific community has shown significant interest in metal diborides ever since the identification of magnesium diboride as a superconductive substance with a critical temperature of 39 K [135, 136].

2.5.1   Bonding and Crystal Structure

The class of transition metal diborides exhibiting an AlB_2 type crystal structure are designated as C32, possessing a space group symmetry of P6/mmm. The hexagonal structure consists of densely packed layers of transition metal, whereby alternate layers are composed of boron and exhibit an identical arrangement to that of graphite [137, 138].

Despite the presence of alternate transition metal (TM) and boron layers, a significant interlayer contact is seen between three adjacent boron atoms and the boron atoms located at the periphery of the hexagonal structure [139].
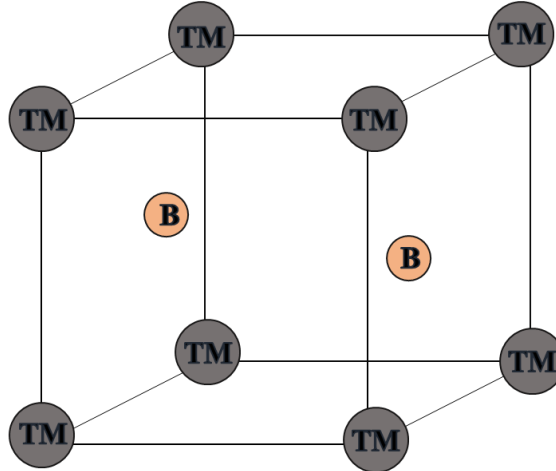
Figure 2.4: Unit Cell of TiB_2

The transition metal atoms are precisely located at the midpoint and central location between two neighboring boron layers. Within this stratified configuration, a singular metallic atom is encompassed by twelve adjacent boron atoms, which are further encircled by six atoms of transition metal. The primordial cell of a crystal possesses a single formula unit, while a crystal exhibiting simple hexagonal symmetry (D6h) is characterized by its structural arrangement [140].

According to reports, the chemical bonding seen within the boron sheets of AlB_2 systems is characterized by covalent bonding. However, in the case of transition metal diborides, the chemical connection between metal and boron atoms exhibits a combination of covalent and ionic bonding. There are conflicting accounts on the nature of the bonding between metal and boron atoms in TiB_2, with some suggesting it is mostly ionic while others propose a covalent character. The bonding and crystal structure of titanium diboride are significant factors that influence the manifestation of distinct physical and chemical characteristics [141].

2.6 Titanium Diboride

The bonding observed in transition metal diborides often includes a combination of metallic, covalent, and ionic chemical connections. The valence electron concentration significantly influences the mechanical characteristics, lattice parameters, and stability of titanium diboride. The bonding and crystal structure of titanium diboride are key factors contributing to its distinctive physical and chemical characteristics [134].
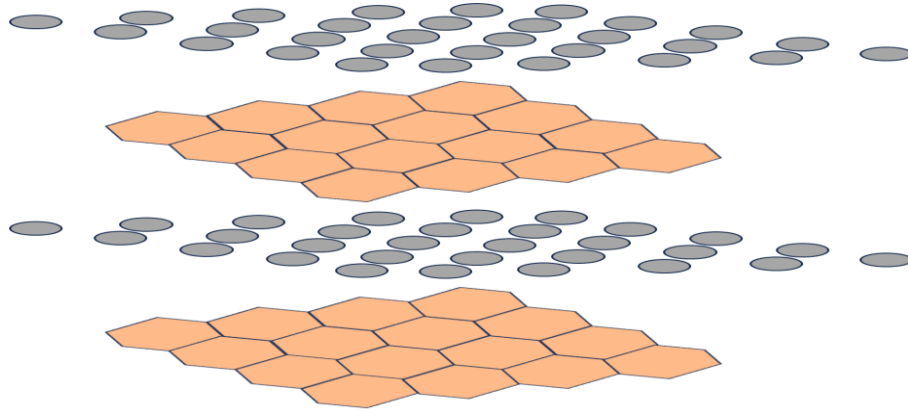
Figure 2.5: Layered Structure inside the Bulk TiB_2

The structure of TiB_2 is classified as AlB_2 type, whereby boron atoms are positioned at 2d (1/3,2/3,1/2) Wyckoff sites, while transition metal atoms are located at 1a (0,0,0) location. This crystal structure belongs to the P6/mmm (No. 191) space group. The AlB_2 structure, characterized by a space group of 191 PG/mmm, was initially documented in the 1930s. This structure consists of boron layers arranged in a hexagonal close-packed configuration, with intervening layers of metals [142]. The hexagonal boron rings are arranged in a stacked configuration, positioned both above and below the metal atoms in a perpendicular orientation to the c-axis [140].

CHAPTER 3: MATERIALS AND METHODS

3.1   Materials

The TiB$_2$ powder utilized in this study was procured from PENSC, China (CAT No. 12045-63-5, purity of 99.9%). This powder served as a bulk titanium diboride (BTB) source throughout the synthesis process of two-dimensional (2D) TiB$_2$. The manufacturer indicated that the particle size was less than 100 μm. The DIW utilized in this study was sourced from HAT Enterprises, a company based in Pakistan. The DIW has a purity level classified as Type II, making it suitable for application as a dispersive medium.

N-Methyl-2-pyrrolidone (NMP), sourced from Merck in Germany, with a CAS number of 872-50-4 and a purity of 99.5%, was employed as the dispersive medium (DM) in the preliminary trials conducted for the synthesis of two-dimensional titanium diboride (2D TiB$_2$).

3.2   Methods

3.2.1   Ultrasonic Parameters

The Ultrasonic Homogenizer system employed in this study was the JY91-IIN N&DN Series, which consisted of a probe US transducer equipped with a US horn, also known as a sonotrode. The experimental setup involved the use of an ultrasonic transducer (UST) in conjunction with a 6 mm-diameter sonotrode (ST) made of titanium alloy. The sonotrode was equipped with a piezoceramic transducer capable of operating at a maximum frequency of 25 kHz and a maximum power of 650 W.

It is worth noting that the sonotrode was operated at 60 to 100% input power during the experiments. This configuration is illustrated in Figure 3.1. The amplitude of ultrasonic waves, measured from the highest point to the lowest point, in this particular configuration reached 30 μm when the input power was at its maximum level of 100%. To ensure effective heat dissipation, a vessel made of stainless steel with a diameter of 60 mm was employed.
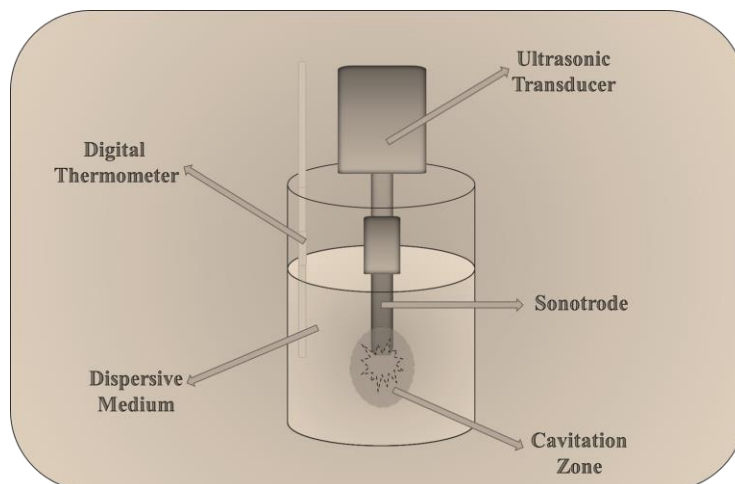
Figure 3.1: Schematic representation of Various components of the ultrasonic configuration employed for the treatment.
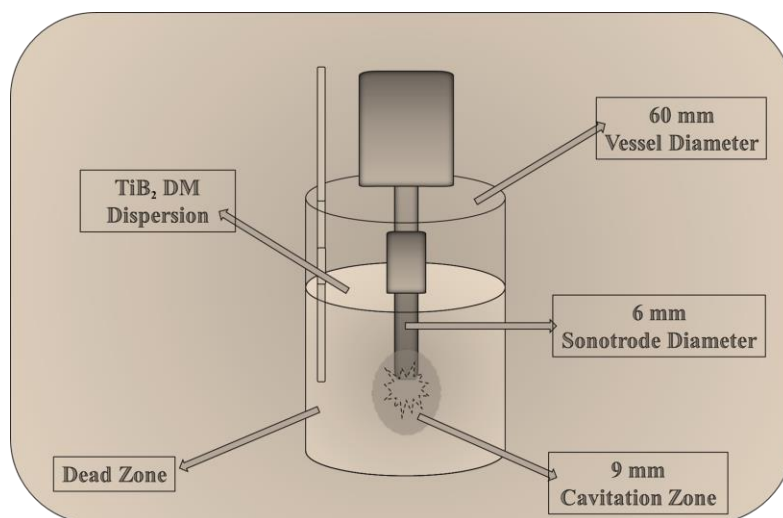
Figure 3.2: The diagram illustrates the relative sizes of the vessel diameter, sonotrode diameter, and cavitation zone.

All studies were conducted using a consistent vessel to ensure uniform application of geometrically input ultrasound waves and to keep a consistent volume of the dispersion medium. The temperature was maintained at a constant level of 40 °C by the utilization of a water bath. The rationale for maintaining the system at the aforementioned temperature is grounded on the enhanced stability exhibited by 2D sheets within this specific temperature range [94, 143, 144].

The interior system's temperature was measured using a DT310LAB digital thermometer equipped with a stainless-steel probe. The dimensions of the cavitation zone (CZ) were seen to be 9 mm in volume or diameter, as depicted in Figure 3.2. This measurement was found to be 1.5 times larger than the diameter of ST [145].
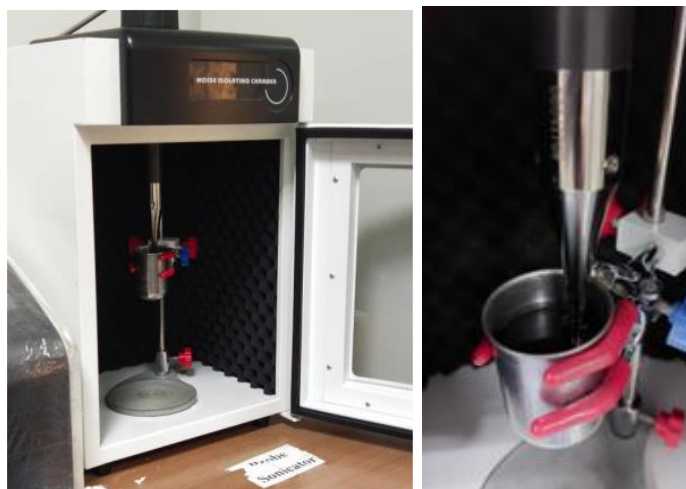
Figure 3.3: Ultrasonic Probe Sonication System Used for the experimentation.

As seen in Figures, the sonotrode was immersed in the liquid at a depth of 15mm below the surface and 20mm above the bottom of the vessel. This positioning ensured that the sonotrode remained centrally located inside the volume of the liquid for all experimental trials, hence maintaining a consistent ultrasonic (US) configuration.

For each experimental setting, a consistent quantity of 1 gram of bulk TiB_2 (BTB) and a uniform volume of 100 milliliters of Dispersion medium (DM) were employed. Pulsed waves with a time interval of 0.2 s in the active state and 0.1 s in the inactive state were utilized to administer ultrasound (US) in order to achieve a uniform dispersion of energy across the cavitation zone (CZ) for all US parameters.

3.3   Effect of Dispersive Medium

In order to assess the impact of the DM, two distinct solvents, namely NMP (often employed) and DIW (a specific DM that was extensively utilized in our experiment), were employed. In a concise manner, the experimentation was partitioned into two distinct

components. In the initial experiment (Ex-1), N-methyl-2-pyrrolidone (NMP) was employed as the dispersing medium.

In the second experiment (Ex-2), deionized water (DIW) is utilized as the dispersing medium (DM). The experiment of DIW was further separated into two distinct components, namely Ex-2a and Ex-2b. The fundamental procedures for both components were the same. The subsequent sections will elaborate on the specific impact of these two decision-making processes.

3.3.1   For NMP

Figure 3.4: Magnetic Stirring Hotplate, Centrifuge and Vacuum Filtration Assembly used in the experimentation.

In Experiment 1, a solution was prepared by dissolving 1 gram of BTB in 100 milliliters of NMP. The dissolution process was facilitated by magnetic stirring for a duration of 1 hour, using a magnetic stirring hotplate (MTops MS300hS) operating at room temperature. The vessel was maintained at ambient temperature for a duration of 18 hours to facilitate the pre-soaking process BTB in N-methyl-2-pyrrolidone (NMP).

This procedure initiates the exfoliation process by subjecting the BTB sheets to presoaking, resulting in the expansion of the sheets. Additionally, this presoaking phase effectively diminishes the interlayer forces inside the BTB material   [95, 96, 146]. Subsequently, ultrasonication is conducted at a power level of 650 W for a duration of 6 hours. The 2D TiB$_2$ material was subsequently subjected to centrifugation in a two-step process.

Initially, the majority of TiB$_2$ was separated using centrifugation, employing the Centurion Scientific C2 Series, at a rotational speed of 500 revolutions per minute for a duration of 30 minutes. During the second phase, the supernatant obtained from the initial centrifugation was subjected to another centrifugation process at a speed of 1000 revolutions per minute for a duration of 30 minutes. This was done in order to eliminate the partially exfoliated two-dimensional titanium diboride (TiB$_2$) material.

The second centrifugation's supernatant was next subjected to vacuum filtering using a rotary vacuum pump (ROCKER) filtration assembly equipped with a Millipore HNWP 0.45 μm filter paper. This process aimed to separate the created 2D TiB$_2$ from the DM.

The filter paper containing the products was subsequently subjected to a drying process in a vacuum oven (VA6033) at a temperature of 70 °C for a duration of 24 hours, resulting in the formation of 2D TiB$_2$. A desiccated specimen of two-dimensional titanium diboride (TiB$_2$) was acquired and designated as sample US-N1.

Figure 3.5: Supernatant After first and second centrifugation.

The subsequent phases of the experiment involved the utilization of ethanol and deionized water (DIW) for the purpose of eliminating the NMP that had become trapped between the sheets. This elimination process was achieved using centrifugation at a speed of 4500 revolutions per minute for a duration of 10 minutes.

Consequently, this experiment may be characterized as a three-step procedure, as seen in the flow chart presented in Figure 3.6. The cleaned sheets were thereafter subjected to a drying process in a specialized oven set at a temperature of 70 °C for a duration of 24 hours. The resulting product was then identified and designated as sample US-N2.
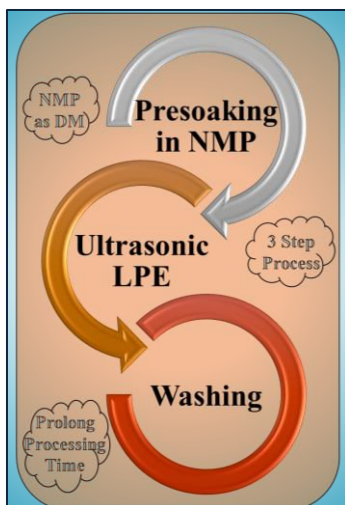
Figure 3.6: The flow chart depicting the Liquid Phase Exfoliation in NMP.

Figure 3.7: Sample US-N1 and US-N2.

3.3.2   For DI Water

Experiment 2 is predicated upon an investigation into the impact of deionized water (DIW) acting as a dispersive medium (DM) during the liquid phase exfoliation (LPE) of two-dimensional titanium diboride (2D TiB_2).

In order to get a deeper understanding of the influence of various US parameters on the synthesis of two-dimensional titanium diboride (2D TiB_2) in a deionized water (DIW) as a dispersive medium (DM), our study is divided into two distinct experimental phases.

In part Ex-2a, the investigation focused on the variety in input powers. In contrast, part Ex-2b examined the variance in the treatment time in the ultrasonic treatment. Further details on these aspects are provided in the subsequent paragraphs.

Figure 3.8: 2D TiB$_2$ solution in supernatant After centrifugation and Dried 2D TiB$_2$ sheets.
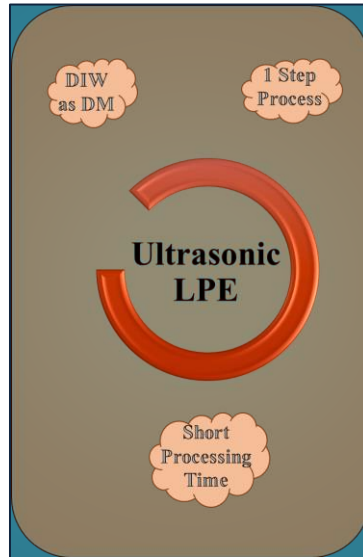
Figure 3.9: The flow chart depicting the Liquid Phase Exfoliation in DI Water.

In both sections of Experiment 2, a quantity of 1 gram of BTB powder was dissolved in 100 milliliters of deionized water (DIW) by agitation for a duration of 20 minutes on a magnetic stirring hotplate set to room temperature. Subsequently, the mixture was transferred to the container, and the characteristics specific to the ultrasonication were modified accordingly, considering whether it pertained to Ex-2a or Ex-2b, as will be elaborated upon in the subsequent sections.

The 2D TiB$_2$ material was isolated from bulk and semi-exfoliated TiB$_2$ by a centrifugation process conducted at a speed of 3000 revolutions per minute for a duration of 10 minutes. Subsequently, the liquid portion was subjected to desiccation within a Petri dish for a duration of 24 hours at a temperature of 70 °C, utilizing a drying oven

manufactured by Memmert. The flow chart in Figure 3.9 demonstrates that exfoliation in DIW has been simplified into a single step process.

3.4 Effect of Ultrasonication Parameters

3.4.1 Effect of Ultrasonication Power

For Ex-2a, the US treatment time at 6 h was fixed, and all other parameters were already fixed as discussed earlier. We changed the US input power, setting it at 3 different points: 390 W (60%), 520 W (80%), and 650 W (100%). The samples were labeled as US-P1 for 390 W, US-P2 for 520 W, and US-P3 for 650 W. The energy density of the acoustic waves is given by Equation 1 [147]. Hence, corresponding energy densities (ED) were 84.24 kJ/mL (390 W), 112.32 kJ/mL (520) W, and 140.40 kJ/mL (650) W.

$$Energy\ Density\ = \frac{Power\ (W) \times Time\ (S)}{Volume\ (L)} \quad JL^{-1} \qquad \ldots\ldots\ldots 1$$

3.4.2 Effect of Ultrasonication Duration

For Ex-2b, the effect of the duration of US treatment was checked by maintaining other parameters constant and fixing the input power at 650 W. We changed the US time in three steps: 6 h (US-T1), 7 h (US-T2), and 8 h (US-T3). The ED of US was 140.40 kJ/mL (6h), 163.80 kJ/mL (7h), and 187.20 kJ/mL (8h).

CHAPTER 4: CHARACTERIZATION

4.1   Instruments

The produced 2D TiB$_2$ samples underwent characterization by the utilization of scanning electron microscopy (SEM), X-ray diffraction (XRD), and atomic force microscopy (AFM). The next section provides an overview of each characterization approach.

4.2   SEM

This approach involves the precise focusing of a narrow electron beam onto the surface of an object. As a consequence, particles such as photons or electrons are dislodged from the surface of the material. Subsequently, the dislodged electrons are directed into the detector for further analysis. The signal generated by the detector causes variations in the luminosity of the cathode ray tube (CRT). At each point of interaction between the beams, a corresponding point is plotted on the cathode ray tube (CRT), resulting in the generation of the material's picture [148].

The interaction between electrons and surfaces results in the emission of secondary electrons (SE), backscattered electrons (BSE), and X-rays [149]. The primary method of detection in scanning electron microscopy (SEM) is through the use of secondary electrons. The emission of these electrons occurs in close proximity to the surface of the sample. Thus, a distinct and lucid representation of the specimen is acquired.

The technique has the capability to discern minute features with dimensions less than 1 nanometer. Moreover, the phenomenon of elastic scattering occurs when input electrons interact with a target material, resulting in the emission of backscattered electrons. Secondary electrons are found at shallower depths compared to primary electrons. The resolution of the given entity is somewhat lower in comparison. When an electron located in the inner shell is dislodged from its orbit, it releases x-rays that possess distinct characteristics [150].

Figure 4.1: SEM (JEOL) present at SCME, NUST.

The utilization of scanning electron microscopy (SEM) is favored due to its convenient sample preparation methods, enabling researchers to examine several aspects of a sample, including its morphology, chemistry, crystallography, and orientation of planes. The scanning electron microscope (SEM) has a variable magnification range spanning from 10 to 500,000 times.

The morphology of the materials can be investigated using the any instrument, and better resolution can be obtained using FESEM. The elemental composition can be

ascertained using an Energy Dispersive X-ray Spectroscopy (EDS) detector that is connected to a Field Emission Scanning Electron Microscope (FESEM).

4.2.1 Sample Preparation

The dimensions of the sheets in the lateral direction were analyzed using a high-resolution scanning electron microscope (SEM) operating at 30 kilovolts (kV) (JEOL-JSM-6490LA). To prepare the sample, a dispersion was created by introducing a nominal quantity of 2D TiB_2, namely 10 mg, into 15 ml of deionized water (DIW).

To achieve a homogeneous dispersion, the mixture underwent sonication in an ultrasonic bath sonicator (WiseClean WUC-A06H) for a duration of 1 hour at ambient temperature. In the context of scanning electron microscopy (SEM) investigation, the samples underwent drop casting, which involved the application of 2 to 3 drops of a finely dispersed 2D TiB_2 material onto a glass surface that had been well cleaned. The specimens were subjected to a drying process within a drying oven, maintained at a temperature of 60 °C, for a duration of 3 hours.

A conductive gold coating with a thickness of a few nanometers was applied onto a two-dimensional (2D) TiB_2 substrate in order to enhance the conductivity of the surface and enable high-resolution imaging. Subsequently, the specimens were subjected to analysis at several levels of magnification, and the most optimal photographs exhibiting superior resolution were captured.

The ImageJ program was utilized for additional image processing and the determination of lateral dimension measures. The identical procedure was employed for the examination of scanning electron microscope (SEM) pictures of the BTB prior to the study of two-dimensional titanium diboride (2D TiB_2).

4.3   XRD

This technique is employed for the purpose of determining the crystal structure of the material. The aforementioned approach is non-destructive in nature and facilitates the

acquisition of Bragg's reflections fingerprints from crystalline materials. The composition is comprised of three primary components. The experimental setup consists of a cathode tube, a sample container, and a detector. X-rays are generated by the process of thermionic emission, wherein a filament element is heated to high temperatures, causing the emission of electrons [151].

Figure 4.2: XRD (BRUKER) present at SCME, NUST.

These electrons are then accelerated towards a target material, where they undergo collisions with the target's electrons, resulting in the production of X-rays.

The structure of crystal is characterized by the presence of distinct layers and planes. An X-ray with a wavelength comparable to the planes in question is reflected at an angle of incidence that is equal to the angle of reflection. The phenomenon of "diffraction" occurs and may be accurately explained by Bragg's Law. [151].

$$2dsin\theta = n\lambda \qquad ....2$$

When Bragg's law is fulfilled, it indicates the occurrence of constructive interference, resulting in the detection of "Bragg's reflections" by the detector. The placements of these reflections provide insights into the inter-layer spacing, whereas ray diffraction analysis informs us about the phase, crystallinity, and purity of the sample.

Through the utilization of this methodology, it is also possible to ascertain lattice misfit, dislocations, and the size of the unit cell. X-ray diffraction experiments were conducted using an X-Ray diffractometer at the School of Chemical and Materials Engineering, National University of Sciences and Technology (SCME-NUST).

4.3.1 Sample Preparation

The X-ray diffractometer (Bruker D2 PHSER diffractometer) was employed to investigate the crystal structure and, notably, to examine the arrangement of 2D TiB_2 sheets along a designated plane. The X-ray diffraction (XRD) analysis provided confirmation of the existence of well-formed two-dimensional (2D) TiB_2 structures, with their orientation aligned parallel to the plane. The samples were analysis using two distinct methodologies in X-ray diffraction (XRD).

In the case of US-BW, US-P390, US-P520, and US-P650, the sample underwent an initial preheating or drying process in a drying oven set at a temperature of 60 °C for a duration of 3 hours. This step was carried out to eliminate any moisture that may have been present or trapped inside the layers of the sample. Subsequently, the desiccated samples were immediately transferred to the stub or sample holder of the X-ray diffraction (XRD) instrument for examination. The identical methodology was employed to examine the X-ray diffraction (XRD) pattern of BTB.

In the case of US-AW, US-T6, US-T7, and US-T8, a quantity of 50 mg of 2D TiB2 was introduced into 15 ml of deionized water (DIW) and subjected to ultrasonication in a bath sonicator for a duration of 1 hour at ambient temperature. Three droplets of the produced solution were deposited onto the cleaned glass substrate.

Subsequently, the substrate is subjected to a vacuum environment within an oven, maintaining a temperature of 70 °C for a duration of 4 hours. Subsequently, the desiccated specimens are carefully positioned into designated sample containers in preparation for examination. The samples were analysis at a range of angles spanning from 5° to 80°, utilizing a slow scan rate.

4.4   AFM

Atomic force microscopy (AFM) is widely regarded as a very sophisticated methodology employed for the examination and characterization of surfaces. This technique is mostly employed for the purpose of assessing surface roughness and analyzing characteristics at the micro and nano scales. The utilization of 2D materials allows for an approximate determination of the dimensions of the sheet, including its length and thickness [152].

Figure 4.3: AFM (JEOL) present at SCME, NUST.

The fundamental idea behind atomic force microscopy (AFM) is the interaction between a sharp cantilever, which is spring-based, and the surface of the specimen. The measurement of force is conducted by observing the deflection of the specimen during scanning [153].Another rationale for employing atomic force microscopy to analyze exfoliated sheets was to assess the aspect ratio (length/thickness), which has significant relevance in subsequent modeling endeavors aimed at investigating gas barrier features.

4.4.1   Sample Preparation

The measurement of the layer thickness was conducted using the JSPM-5200 JEOL scanning probe microscope (SPM) with a very precise probe. Atomic forces were employed to generate a three-dimensional picture. The utilization of atomic force microscopy (AFM) in contact mode, characterized by its high-resolution capabilities, enables the determination of sheet thickness.

A dispersion preparation was conducted by adding 5 mg of 2D TiB_2 to 15 ml of deionized water (DIW) and subjecting it to ultrasonication at room temperature for a duration of 1 hour. A single droplet of the produced dispersion was applied over a smooth and polished Si/SiO_2 surface, which exhibited little roughness. The specimen was subjected to a desiccation process within a vacuum oven, whereby it was exposed to a temperature of 70 °C for a duration of 4 hours. Subsequently, the processed samples were introduced into a vacuum chamber and subjected to individual scanning using an AFM.
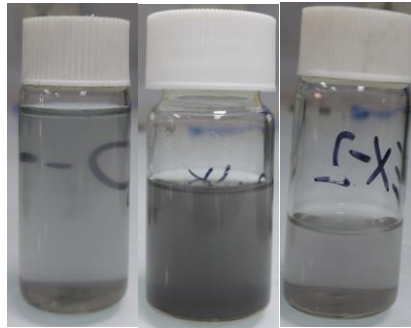
Figure 4.4: Different Dispersions for SEM, XRD and AFM.

CHAPTER 5: RESULTS AND DISCUSSION

5.1 Analysis of Bulk TiB$_2$

Prior to conducting the investigation of our two-dimensional Titanium Diboride (2D TiB$_2$) material, we performed an examination of the Bulk Titanium Diboride (BTB) compound using scanning electron microscopy (SEM) and X-ray diffraction (XRD) techniques.

5.1.1 SEM Analysis of BTB

The findings obtained from the scanning electron microscopy (SEM) analysis indicated that the BTB sample exhibited an average particle size ranging from 50 μm to 100 μm, as visually shown in Figure 5.1. The particles exhibited varying morphologies characterized by either rough or smooth surfaces and possessed multilayer structures.
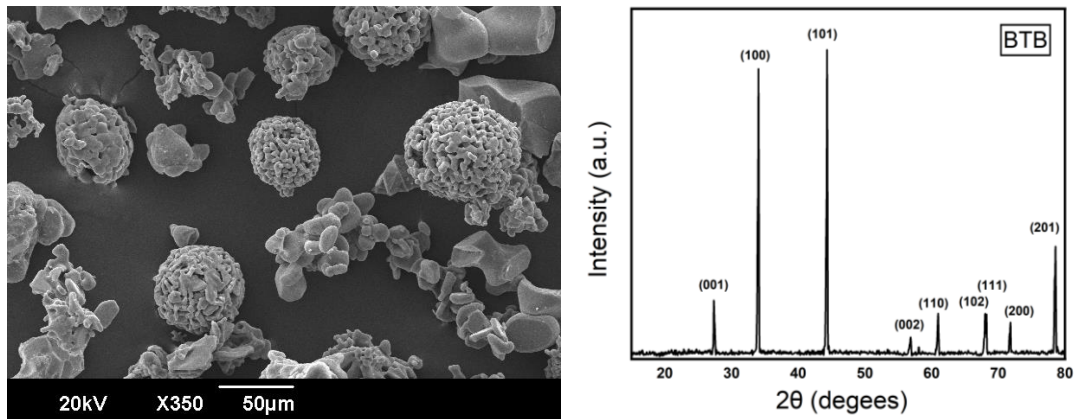
Figure 5.1: SEM image and XRD of Bulk TiB$_2$

5.1.2 XRD Analysis of BTB

The X-ray diffraction (XRD) analysis revealed that BTB exhibited a hexagonal crystal structure characterized by a P6/mmm space group. The diffraction pattern exhibited distinct peaks corresponding to various crystallographic planes. Specifically, a minor peak

was observed for the (001) plane at an angle of 27.5°, a prominent peak was observed for the (100) plane at an angle of 34.1°, and the most intense peak was observed for the (101) plane at an angle of 44.4°.

Additionally, smaller, or less significant peaks were observed for the (002) plane at an angle of 56.9°, the (110) plane at an angle of 61.1°, the (102) plane at an angle of 68.1°, the (111) plane at an angle of 68.3°, the (200) plane at an angle of 71.904°, and the (201) plane at an angle of 78.6°. These observations are depicted in figure 5.1 of the BTB. The acquisition of this pattern was compared by the utilization of the JCPDS Card No. 01-075-1045.

5.2   Effect of Dispersive Medium on 2D TiB$_2$

The present study aimed to evaluate the impact of various dispersion mediums on the synthesis of 2D TiB$_2$. This was accomplished via the utilization of scanning electron microscopy (SEM) and X-ray diffraction (XRD) techniques. The findings will be examined and analyzed in the subsequent sections.

5.2.1   Analysis of LPE in NMP

In Experiment 1, the use of N-Methyl-2-pyrrolidone (NMP) was employed as a dispersing medium. The production of two-dimensional titanium diboride (2D TiB$_2$) in N-methyl-2-pyrrolidone (NMP) included a sequential procedure, as documented in references [95, 96, 146]. The product samples were partitioned into two distinct segments. The US-N1 was not subjected to a cleaning process.

5.2.2   SEM Analysis of Sample US-N1

The scanning electron microscopy (SEM) pictures presented in Figure 5.2 demonstrate the self-assembly of NMP on US-N1 sample 2D sheets substrate following the process of drop casting and subsequent drying of the dispersion on a glass surface [144, 154, 155]. Therefore, the observation of 2D TiB$_2$ through scanning electron microscopy

(SEM) for the US-N1 sample was hindered due to the inadequate elimination of N-methyl-2-pyrrolidone (NMP) from nanosheets [156, 157].
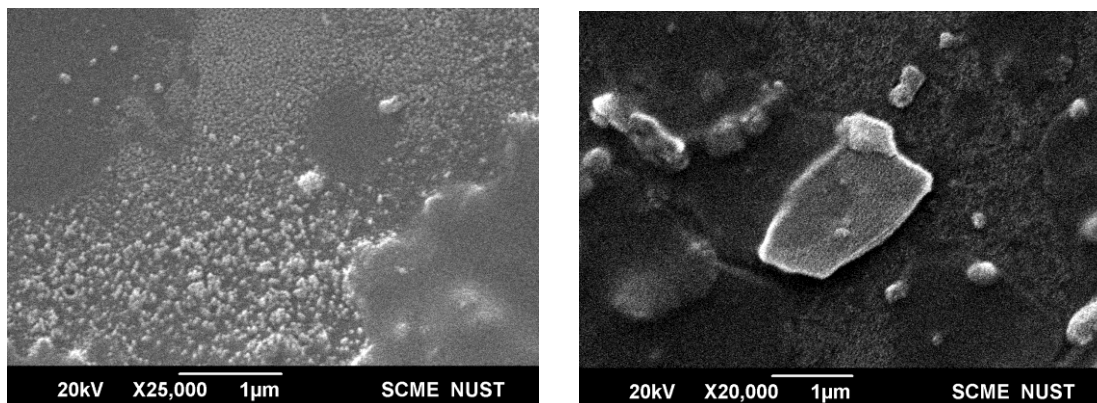
Figure 5.2: SEM image of Sample US-N1 and US-N2

5.2.3   SEM Analysis of Sample US-N2

To eliminate the NMP and contaminants, we subjected our sheets (US-N2) to a washing procedure, resulting in an augmentation of both the synthesis stages and the processing time. Following the washing procedure, the produced 2D sheets were visible. However, it is important to note that the washing process introduced additional complexity to the liquid phase exfoliation (LPE) in N-methyl-2-pyrrolidone (NMP), transforming it into a three-step procedure. The SEM image of US-N2 is depicted in Figure 5.2. The picture reveals that the lateral dimensions of the 2D TiB_2 in sample US-N2 range from 1 μm to 2 μm. Nevertheless, remnants of NMP [144, 157] were still evident, as seen in Figure 20.

5.2.4   XRD Analysis of Sample US-N1

The X-ray diffraction (XRD) data presented in Figure 5.3 indicates that, in the case of US-N1, there is an increase in the intensity of the (001) plane peak at an angle of 27.3°, accompanied by a little shift (27.5° for bulk TiB_2). Additionally, the intensities of the primary peaks corresponding to the (100) and (101) planes at angles of 34.0° and 44.3° respectively, exhibit a reduction. The intensity of all remaining peaks exhibited a decline. The observed variation in intensities can be attributed to the alignment of sheets along

specified planes, which in turn resulted in the occurrence of strong diffraction [158]. A little alteration in the X-ray diffraction (XRD) pattern of US-N1 was observed in comparison to the XRD pattern of bulk TiB_2.
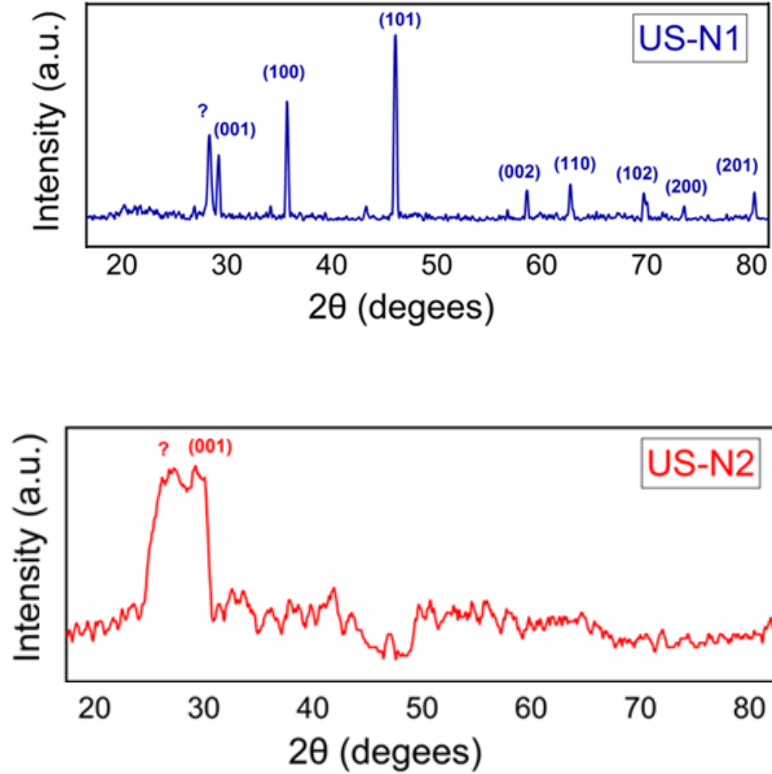
Figure 5.3: XRD Pattern of Sample US-N1 and US-N2

Additionally, a little increase in the width of the US-N1 X-ray diffraction (XRD) peaks was observed. The displacement of the peaks observed can be attributed to the mechanical forces generated by ultrasonication, which facilitated the process of exfoliation throughout the range of [159-162]. The d-spacing experienced modest alterations or enhancements due to the influence of these forces, wherein ultrasonic forces attenuated the out-of-plane forces, resulting in the exfoliation of the sheets. Consequently, a minor shift towards lower angles was seen in the X-ray diffraction (XRD) pattern. The phenomenon of peak widening occurs while transitioning from bulk to nano scale, resulting in a reduction of diffraction planes [158, 163, 164].

The X-ray diffraction (XRD) findings provide conclusive evidence of the successful synthesis of two-dimensional (2D) titanium diboride (TiB_2). The obtained XRD patterns indicate that the 2D TiB_2 sheets are oriented along the (001) crystallographic plane, with an inclination angle of 27.3°. Nevertheless, an additional peak at 26.6° was seen, suggesting the existence of impurities within the 2D TiB_2 material. During the synthesis process in NMP, it is possible for contaminants to be integrated into the 2D TiB_2 material. The contaminants in question were found to be either pre-existing in NMP and BTB or capable of being generated during the LPE process [60, 165-167].

Nevertheless, the X-ray diffraction (XRD) pattern of BTB indicated the absence of contaminants in the bulk powder. Therefore, it can be inferred that these impurities must have originated from two other sources. Moreover, pure N-methyl-2-pyrrolidone (NMP) was employed, hence potentially leading to additional plane expansion because of NMP entrapment inside the exfoliated sheets of two-dimensional titanium diboride (TiB_2).

5.2.5 XRD Analysis of Sample US-N2

The X-ray diffraction (XRD) pattern of US-N2, as seen in Figure 5.3, provides confirmation of the successful synthesis of two-dimensional (2D) TiB_2. This confirmation is evident from the presence of a single strong peak observed at an angle of 26.8°, corresponding to the (001) plane. The observation of a peak shift of 0.7° for the (001) plane, accompanied by diminished intensities of all other planes, provides confirmation of the successful synthesis and precise alignment of two-dimensional TiB_2 along the (001) plane [17, 168]. The causes of Peak shift and Peak Broadening seen in the sample US-N1 are consistent with those previously described, therefore confirming the presence of a limited number of 2D TiB_2 layers [169, 170]. A residual signal at 24.9° was observed, indicating the continued presence of contaminants and N-methyl-2-pyrrolidone (NMP) inside the sheets [60, 165-167, 171].

5.2.6 Effect of NMP

Therefore, it was determined by the utilization of scanning electron microscopy (SEM) and X-ray diffraction (XRD) that the presence of N-methyl-2-pyrrolidone (NMP)

and impurities, which were introduced during the synthesis process, persisted even after undergoing post-treatment and washing procedures, as previously stated in experimental studies [144].

To achieve the total elimination of N-Methyl-2-pyrrolidone (NMP), it is necessary to subject the substance to prolonged drying at elevated temperatures [172, 173].

The elimination of impurities can be achieved by the process of annealing, which involves subjecting the material to high temperatures [174-176]. The inclusion of additional steps such as further drying or annealing in the already existing three-step process of LPE utilizing NMP as a dispersive medium (DM) would result in increased time consumption and complexity. The applicational qualities of 2D TiB$_2$ as a product may be influenced by the presence of NMP or impurities.

5.2.7 *Analysis of LPE in DI Water*

To address the challenges connected with NMP, the decision was made to substitute the DM with deionized water (DIW) and subsequently synthesis 2D TiB2. The utilization of US cavitation in pure deionized water (DIW) BTB solutions is solely used as a unique one procedural step for the exfoliation process of two-dimensional titanium diboride (TiB$_2$).

A previously described technology of LPE like our study was utilized for graphene, in which a unique and customized equipment was utilized to test solutions containing water-based surfactants in a restricted volume [90]. Additionally, a comparable investigation was conducted to examine the utilization of LPE [104] for the industrial-scale synthesis of graphene. The management of lateral dimension, layer thickness, and concentration of the 2D dispersion is primarily achieved by the manipulation of two important factors, namely the US input power and US duration in the LPE [97].

The present work presents a manufacturing procedure for the exfoliation of 2D TiB$_2$ in pure deionized water (DIW). This process is notable for its cleanliness, environmental friendliness, and possible scalability. Significantly, this procedure does not entail the

utilization of any chemical additives. The confirmation of the presence of a two-dimensional (2D) TiB_2 material has been achieved through the utilization of several characterization techniques.

In addition, we conducted the synthesis process utilizing the specified parameters of NMP. Furthermore, we undertook optimization of crucial factors, such as ultrasonication (US) input power and treatment duration. It is worth noting that, to the best of our knowledge, no other work has explored these parameters for 2D TiB_2. The next section presents a discussion of the outcomes obtained from all tests conducted with deionized water (DIW) as the dispersing medium (DM).

5.3   Effect of Input Power

5.3.1   At 390 W Power

To investigate the impact of input power (Ex-2a) on the system under study (US), we maintained the consistency of all other parameters. Specifically, we utilized a sonotrode with a consistent diameter, employed the same configuration for the experimental setup, and employed deionized water (DIW) as the designated medium (DM). The initial power capacity harnessed in the US was 390 watts.

5.3.2   SEM analysis of Sample US-P1

The scanning electron microscopy (SEM) picture presented in Figure 5.4 reveals that the typical lateral dimensions of the observed structures are around 10 μm, while their layer thickness is larger than 100 nm, or even 0.2 μm. The sheets included a total of more than one hundred layers. The ratio between the lateral dimension and the layer thickness was around 34 [177].

At a power level of 390 W, it was observed that the cavitation field (CF) did not exhibit sufficient strength, and the energy density (ED) was not sufficiently high to facilitate the desired intercalation-controlled delamination (ICD) process for the

exfoliation of 2D TiB$_2$. Therefore, the atomic force microscopy (AFM) analysis of US-P1 was not conducted due to its thickness falling beyond the nano range
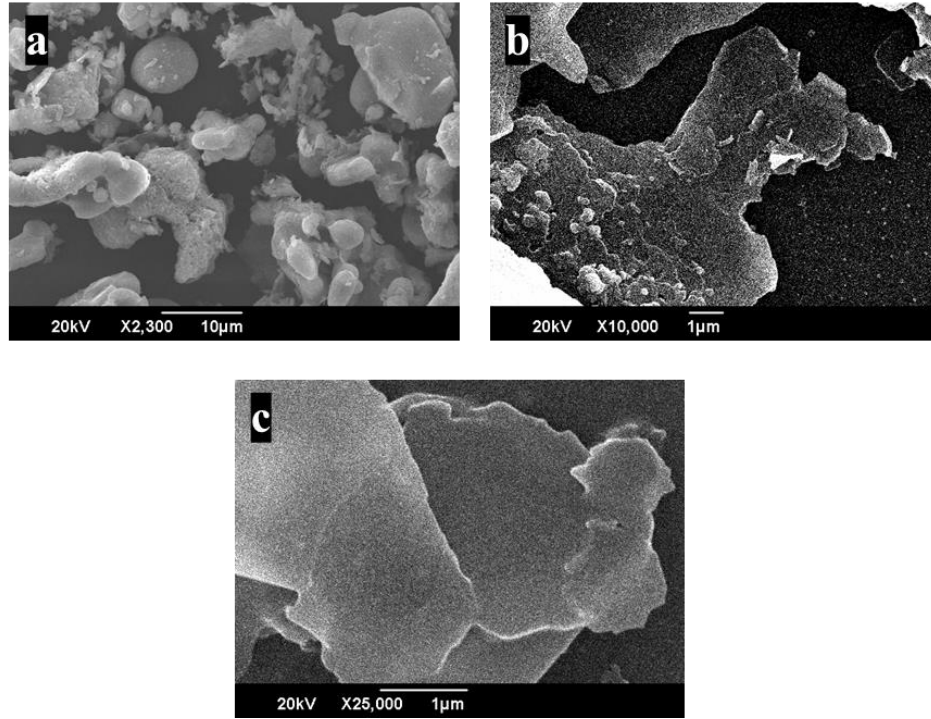
Figure 5.4: Comparative SEM of the samples US-P1 (a), US-P2 (b) and US-P3 (c)

5.3.3 XRD analysis of Sample US-P1

The X-ray diffraction (XRD) findings depicted in Figure 5.5 demonstrate that in the case of sample US-P1 (390 W), the intensity peak corresponding to the (001) plane exhibited a rise, accompanied by a shift of 26.9° (with a 0.6° deviation from the BTB peak). The intensity of the primary peak of BTB is seen to drop [161, 178] at the angles of 34.1° and 44.4° for the crystallographic planes (100) and (101), respectively.

A marginal decline in the magnitudes of all remaining peaks was observed. No notable increase in peak broadening or peak shifting was seen in the other planes, which is a prerequisite for transitioning from the bulk to the nanoscale regime [179]. Based on the absence of this prominent factor, it may be inferred that there was a lack of substantial exfoliation observed at the power level of 390 W.
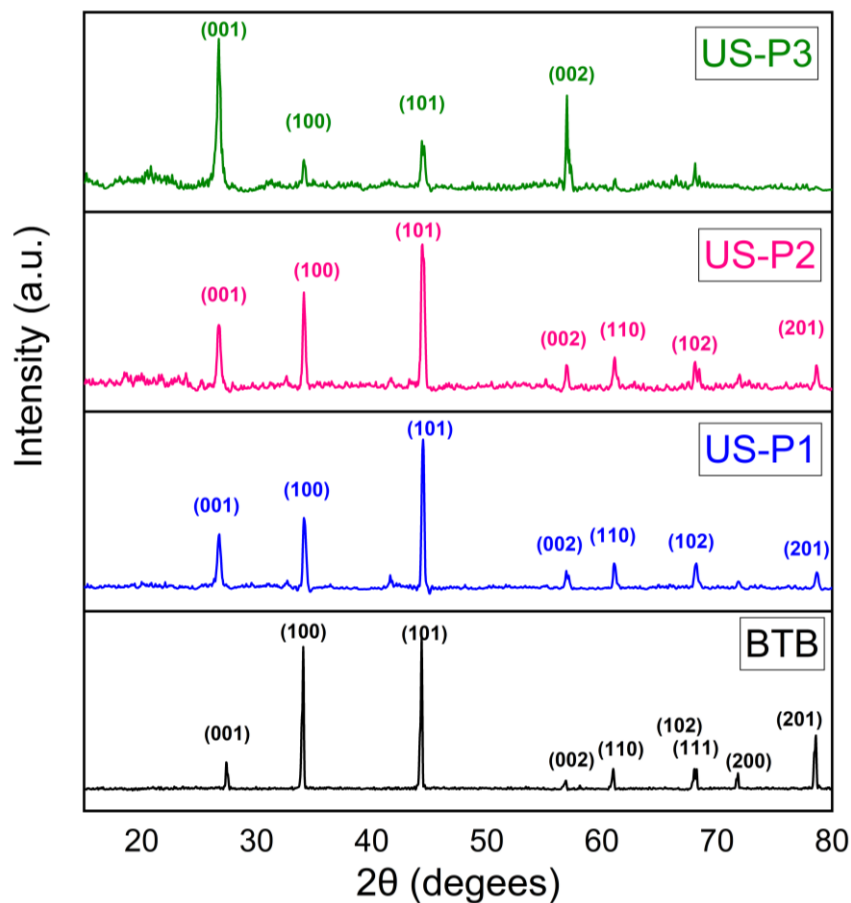
Figure 5.5: Comparative XRD patterns of the samples BTB, US-P1, US-P2 and US-P3

5.3.4 At 590 W Power

The power input for the second experiment conducted in the Ultrasonic treatment to synthesize 2D TiB_2 utilizing DI water as the dispersing medium was 520 W.

5.3.5 SEM analysis of Sample US-P2

The scanning electron microscopy (SEM) picture presented in Figure 5.4 reveals that sample US-P2 (520 W) exhibits lateral dimensions ranging from about 5 μm to 8 μm. Multiple sheets were seen, each with distinct lateral dimensions, with an average lateral dimension of 6 μm. The scanning electron microscopy (SEM) pictures revealed the

presence of a well-defined sheet-like structure, indicating the sufficient extent of exfoliation of the two-dimensional (2D) TiB$_2$ material [180].

5.3.6   XRD analysis of Sample US-P2

The X-ray diffraction (XRD) pattern of US-P2, as seen in Figure 5.5, exhibited a notable shift in the peak corresponding to the (001) plane, which occurred at an angle of 26.8°. Additionally, the strength of this peak saw a further rise, which may be attributed to the sheets being perfectly aligned along this plane [170, 181]. In the sample US-P2, the planes (100) and (101) exhibited a minor shift in the primary peaks of the BTB, measuring around 34.05° and 44.35°, respectively.

The observed drop in the intensity of these planes indicates a substantial reduction in layer thickness, consistent with findings from previous research [182]. Additionally, a little displacement was seen in all other peaks, accompanied by a drop in their respective intensities, except for the (002) plane peak at an angle of 56.85°. This observation further substantiates the hypothesis about the alignment of sheets along the (001) plane. A phenomenon of peak widening was seen across all peaks, indicating a substantial level of cavitation intensity (CI) at 520 W, resulting in the exfoliation of the 2D TiB$_2$ from BTB with layer thicknesses below 100 nm or within the nano-scale range [183].

5.3.7   AFM analysis of Sample US-P2
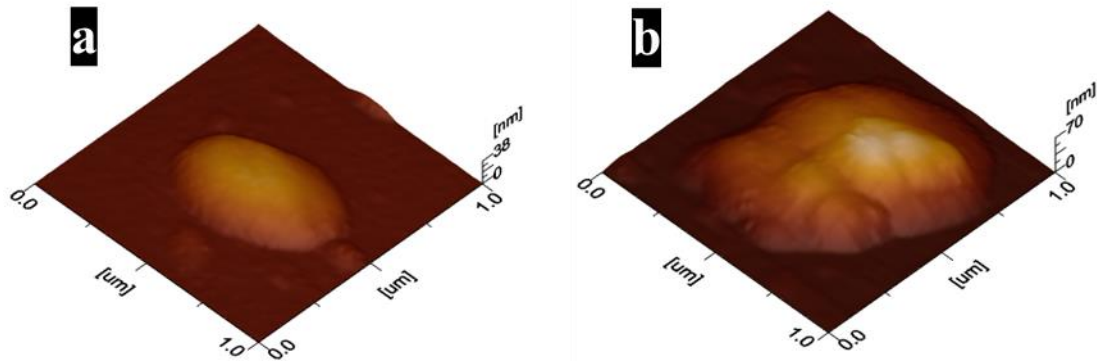
Figure 5.6: Comparative SEM of the samples US-P2 (a) and US-P3 (b)

43

Moreover, to determine the thickness of the layer, Atomic Force Microscopy (AFM) was conducted, as seen in Figure 5.6. The atomic force microscopy (AFM) pictures revealed a layer thickness of approximately 68 nm, indicating the presence of roughly 140 to 150 layers of TiB_2 within the sheets [142, 184]. The ratio between the lateral dimensions and layer thickness of was found to be 88, which exceeds that of US-P1 [177]. At a power level of 520 W, the energy density (ED) was sufficient to generate a cavitation field (CF) capable of delivering an appropriate dosage of inertial cavitation (ICD). However, the intensity of the CF remained insufficient to achieve a desired level of sheet thickness [64].

5.3.8 At 650 W Power

In the subsequent round of the experiment investigating the impact of input US power, the value was further augmented to 650 W.

5.3.9 SEM analysis of Sample US-P3

The appropriate 2D sheets may be observed in Figure 5.4's scanning electron microscope (SEM) picture. The lateral diameters of the sheets were around 5 micrometers. The sheets exhibit no curling or bending. Therefore, at a power level of 650 watts, an adequate amount of intercalation and delamination (ICD) was facilitated by the energy density, resulting in a sufficiently strong cavitation field that effectively exfoliated the sheets [90]. The cavitation zone (CZ) exhibited a high degree of homogeneity, resulting in a limited range of lateral dimensions with a little size distribution [185].

5.3.10 XRD analysis of Sample US-P3

The X-ray diffraction (XRD) pattern depicted in Figure 5.5 demonstrates that the strength of the (001) peak in US-P3 has notably grown, surpassing all other peaks. This indicates that a significant portion of the sheet is now aligned along the (001) plane, inclined at an angle of 26.6°.

Additionally, there is a minor shift in the peak position compared to the BTB [170, 181]. The second most intense peak was seen in the (002) plane, exhibiting a little angular

shift of 56.75°. Additionally, the primary peak of BTB in the (100) and (101) planes had insignificant intensities, accompanied by a minor angular displacement. The disappearance of all the remaining peaks may be attributed to the alignment of the manufactured nanosheets in a precise direction along the plane [182]. The observed peaks exhibited substantial widening, suggesting the existence of two-dimensional (2D) TiB2 with very thin dimensions on the order of nanometers [183].

In the present study, a significant proportion of the two-dimensional titanium diboride (TiB$_2$) samples exhibited alignment predominantly along the (001) crystallographic plane. The observed reduction in the magnitude of prominent peaks indicates the presence of a limited number of stratified 2D TiB$_2$ [186].

5.3.11 AFM analysis of Sample US-P3

The atomic force microscopy (AFM) picture seen in Figure 5.6 provided evidence indicating that the layer possessed a thickness of about 35 nm. The 2D TiB$_2$ exhibited a notable presence of around 70 to 80 layers [142, 184]. The current ratio between the lateral dimensions and layer thickness is 145 [177].

In the case of the US-P3 sample, the Energy density (ED) operating at a power level of 650 W exhibited a significant intensity, resulting in the generation of a pronounced cavitation field (CF) within the cavitation zone (CZ) of the sonotrode [90].

The experimental procedure yielded 2D TiB$_2$ sheets of great purity, characterized by a limited number of layers. The density of the 2D sheets within the dispersive medium exhibited a notable level of concentration.

5.4   Effect of Treatment Time

In Experiment 2b (Ex-2b), the objective was to examine the impact of the length (time) of the ultrasonic treatment. To align with the inquiry focused on power dependency, the input power was held constant at 650 W. All remaining parameters, setup

configurations, and the diameter of the sonotrode were held constant, and all experimental procedures were conducted using deionized water as the dispersing medium.

The duration of the cavitation intensity (CI) given by the cavitation field (CF) of the sonotrode was altered by manipulating the ultrasonic treatment period. The alteration in cavitation intensity resulted in a modification of the energy density, thereby affecting the intensity of ICD inside the cavitation zone [147].

5.4.1   For 6 h Treatment

The implementation of time study commenced with the first selection of a 6-hour treatment duration in the Ultrasonication. While the impact of this phenomenon has been somewhat examined in the context of US-P3, the samples (US-T1) utilized in this study were freshly produced, and the analytical techniques employed were enhanced.

5.4.2   SEM analysis of Sample US-T1
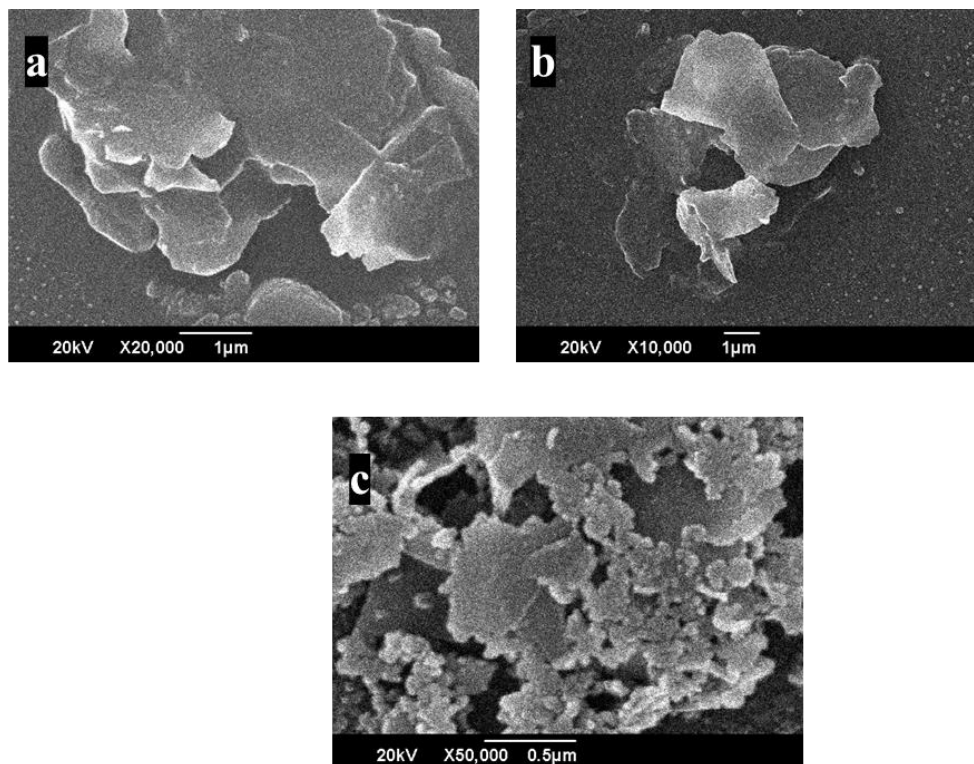
Figure 5.7: Comparative SEM of the samples US-T1 (a), US-T2 (b) and US-T3 (c)

The scanning electron microscopy (SEM) picture presented in Figure 5.7 illustrates the presence of two-dimensional (2D) sheets of titanium diboride (TiB_2) in sample US-T1 (6 h). These sheets exhibit lateral dimensions of about 5 μm. The lateral dimensions of the sheets exhibit a highly limited distribution. The sheets exhibited no structural irregularities, as evidenced by the absence of any curling or bending.

This finding indicates that the effective dose (ED) of the CZ (chemical compound) supplied an adequate amount of intercalation compound (ICD), resulting in a significant level of exfoliation [90].

In this instance, the concentration of the 2D titanium diboride (TiB_2) sheets in the deionized water (DIW) as the dispersing medium (DM) was seen to be significantly elevated.

5.4.3   XRD analysis of Sample US-T1

The X-ray diffraction (XRD) plot presented in Figure 5.8 demonstrates that sample US-T1 exhibits a solitary and prominent peak at an angle of 26.1°, corresponding to the (001) plane. Furthermore, this peak is observed to have undergone a shift of 1.4°.

The observed phenomenon of peak shifting can be attributed to the expansion of the planes inside the layers of two-dimensional TiB_2 sheets, which is caused by the pressures exerted during sonication [170, 181].

The observed phenomenon of peak broadening indicates that the thickness of the layers falls inside the nanometer scale, specifically denoting that the sheets are extremely thin with a limited number of layers [183].

The suppression of all other peaks was seen for all other planes. The obtained findings indicate the presence of a limited number of densely stacked two-dimensional (2D) sheets of TiB_2, exhibiting a precise alignment with the (001) plane [182].

Figure 5.8 shows the comparative XRD patterns of the samples BTB, US-T1, US-T2 and US-T3.
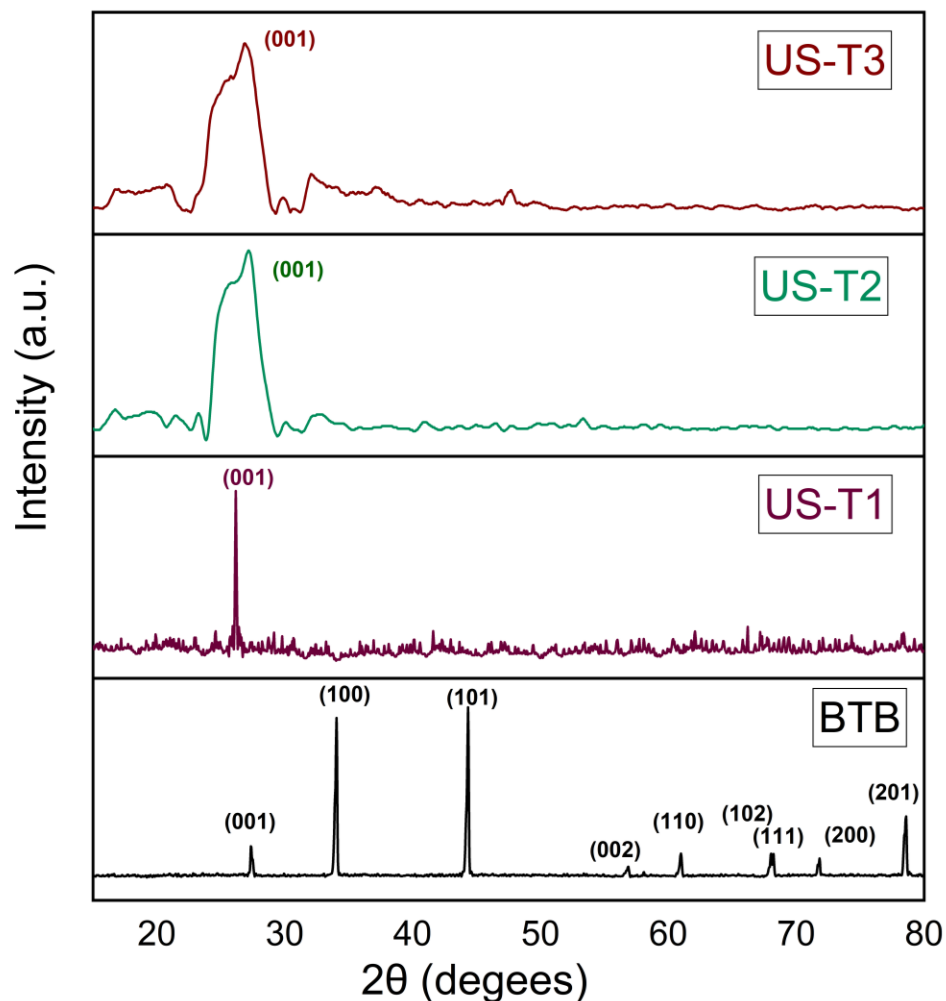
Figure 5.8: Comparative XRD patterns of the samples BTB, US-T1, US-T2 and US-T3

5.4.4   AFM analysis of Sample US-T1

The AFM picture depicted in Figure 5.9 provided confirmation that the mean thickness of the sheets was around 34 nm, indicating the presence of 68 to 77 layers inside the sheets [142, 184]. The lateral-to-layer thickness ratio was around 148 [177]. Therefore, the Cavitation Intensity (CI) of the Cavitation Field (CF) proved to be sufficient for a duration of 6 hours to surpass the intermolecular forces acting between the layers. Consequently, we successfully generated two-dimensional sheets consisting of just a small number of layers.
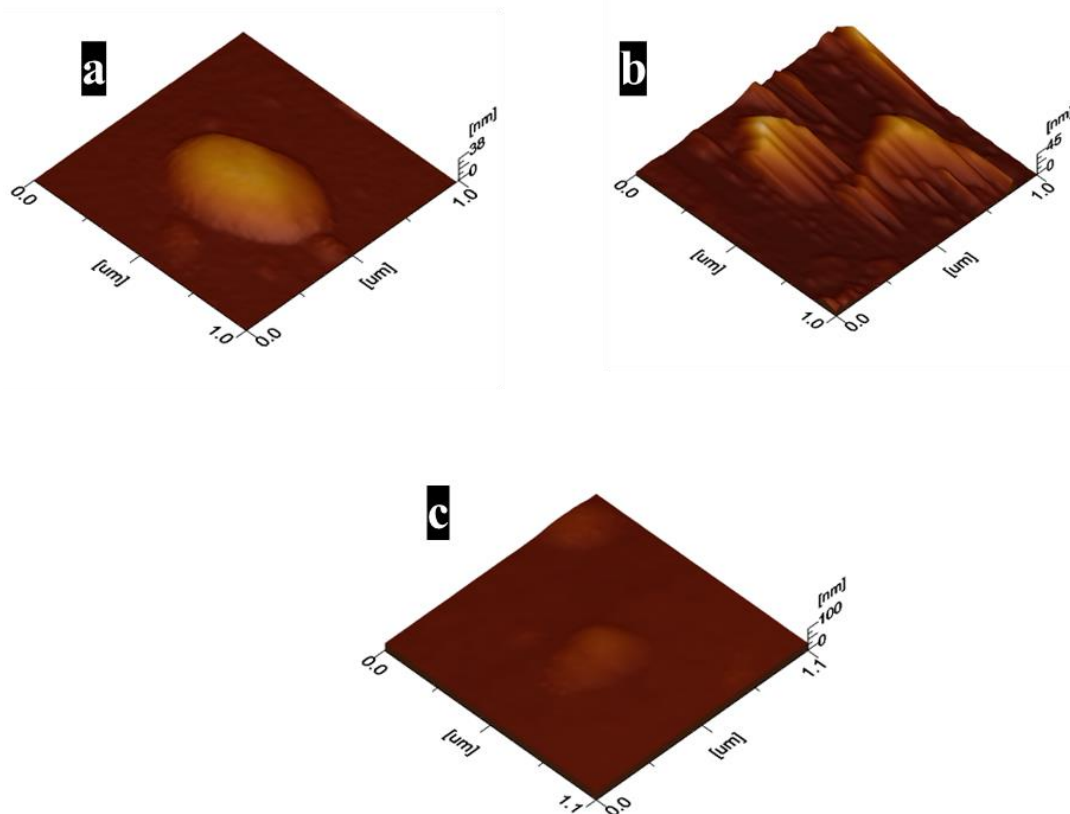
Figure 5.9: Comparative AFM of the samples US-T1 (a), US-T2 (b) and US-T3 (c)

5.4.5   For 7 h Treatment

To assess the impact of varying durations of ultrasonic treatment, our trial was extended to a period of 7 hours.

5.4.6   SEM analysis of Sample US-T2

The scanning electron microscopy (SEM) picture depicted in Figure 5.7 illustrates that for the US-T2 sample, the lateral dimensions experienced a reduction to a range of 2 to 4 μm, with an average size of 3.5 μm. The observed decrease in the lateral dimension

indicates that the Cavitation Field (CF) is now exhibiting signs of lateral fracture in addition to changes in thickness.

The sheets exhibited no discernible faults or contaminants of notable consequence. The density of the sheets was also significantly increased. The lateral dimensions experienced breakage because of the high Inertial Cavitation Dosage (ICD) given by the Energy Density (ED) in the CZ. Prolonged exposure to this high ICD resulted in the breaking of both the lateral dimensions and the thickness of the sheets [104, 147].

5.4.7 XRD analysis of Sample US-T2

The X-ray diffraction (XRD) pattern of sample US-T2 is depicted in Figure 5.8. The graph illustrates a prominent and wide peak observed in the (001) plane. The peak exhibited an angle of 25.9°, which represents a deviation of 1.6° when compared to the peak of BTB. The observed phenomenon of peak broadening indicates that the thickness of the layers falls inside the nanometer scale, namely, the sheets consist of just a few layers [183]. The observed change in the angle indicated the expansion of the planes because of the shear forces experienced during ultrasonic cavitation [170, 181].

The observed singular and highly pronounced peak indicate the exceptional alignment of the sheets along the (001) plane [182]. The presence of an asymmetric peak can be attributed to the existence of sheets with varying lateral diameters, resulting in a significantly broader distribution [187, 188]. The influence of lateral dimensions on d-spacing is more pronounced in sheets with larger dimensions, resulting in a greater shift and the formation of a single broad asymmetric peak [104, 189]. In contrast, sheets with lower lateral dimensions have a lesser effect on d spacing.

5.4.8 AFM analysis of Sample US-T2

The atomic force microscopy (AFM) picture depicted in Figure 5.9 demonstrated a reduction in the average layer thickness to about 31 nm. Consequently, the quantity of sheets in the 2D sheets has been augmented to a range of 60 to 65 sheets [142, 184]. The

ratio of lateral dimension to layer thickness showed a decline, namely from 148 (in the US-T1 sample) to 110 (in the US-T2 sample) [177].

Based on the observed data, it can be inferred that during a duration of 7 hours, there was a decrease in the thickness of the sheet material. Additionally, a few thick sheets were found to be layered. However, during this specific treatment period, the energy density (ED) exhibited a very high intensity, resulting in a prolonged duration of inertial cavitation dosage (ICD). Consequently, this high ICD caused the lateral dimensions of the material to fracture [64, 185].

5.4.9   For 8 h Treatment

When we extended the duration of treatment to 8 hours, there was an observed increase in the impact of energy density on the lateral dimensions.

5.4.10 SEM analysis of Sample US-T3

The SEM picture of sample US-T3 (8 h) is depicted in Figure 5.7. The lateral dimensions were decreased to around 1 micrometer. The 2D TiB_2 sheets that were generated exhibit structural faults, with most of these defects being associated with the edges. Based on the observations, it can be inferred that the 8-hour therapy resulted in an elevated ED, leading to a notably heightened CF inside the CZ. The coefficient of friction in this field was sufficiently elevated to cause both the peeling off of the sheets and the fracturing of those that were manufactured during 8 hours treatment [90, 104].

5.4.11 XRD analysis of Sample US-T3

The X-ray diffraction (XRD) pattern of sample US-T3, as seen in Figure 5.8, has a very wide and strong peak corresponding to the (001) plane. This peak is observed to have a little deviation of 2.0° when compared to the peak of BTB, which is detected at an angle of 25.5°. The observed shift in the peak indicates a decrease in the thickness of the layers, which may be attributed to the amplification of shear forces acting on the planes.

Consequently, there is a little expansion of the planes inside sheets [170, 181]. The observed peak widening at the specified angle indicates that the lateral dimensions of the sample began to deteriorate during the 8-hour treatment period [158, 163, 164]. The presence of an asymmetric peak indicated the existence of sheets with varying lateral diameters, exhibiting a considerably broader dispersion [187, 188]. Consequently, there is a concomitant decrease in the lateral dimensions [104, 189].

5.4.12 AFM analysis of Sample US-T3

The atomic force microscopy (AFM) examination depicted in Figure 5.9 demonstrated that the mean thickness of the layer had been diminished to around 21 nm, corresponding to an estimated 40 to 44 layers of TiB_2 [142, 184]. However, there has been a dramatic reduction in the ratio of lateral dimensions to layer thickness, presently standing at 47 [177]. The Energy density (ED) generated a substantial inertial cavitation dosage (ICD) within the cavitation zone (CZ). The cavitation intensity (CI) exhibited a substantial magnitude, and when this phenomenon persisted over an extended period, it resulted in the disruption of the lateral dimensions [177].

5.5   Comparison of Samples prepared in DI Water and NMP

The comparative analysis of N-methyl-2-pyrrolidone (NMP) and deionized water (DIW) as dispersive media for the Ultrasonic treatment of titanium diboride (TiB_2) may be approached from two distinct perspectives. Figure 5.10 depicts the flow chart illustrating the process of Liquid Phase Exfoliation (LPE) conducted in both dispersion mediums (DMs).

The graphic illustrates that the liquid phase exfoliation (LPE) procedure in N-methyl-2-pyrrolidone (NMP) as the designated solvent was comprised of three distinct steps. Additionally, several sub-steps were involved within these three primary processes, resulting in a protracted, significantly time-consuming, and arduous procedure. In contrast, the LPE procedure in DIW, functioning as DM, was executed as a singular phase. The LPE procedure described herein is characterized by a streamlined process consisting of a limited

number of sub-steps, resulting in a rapid, straightforward, and cost-effective implementation.
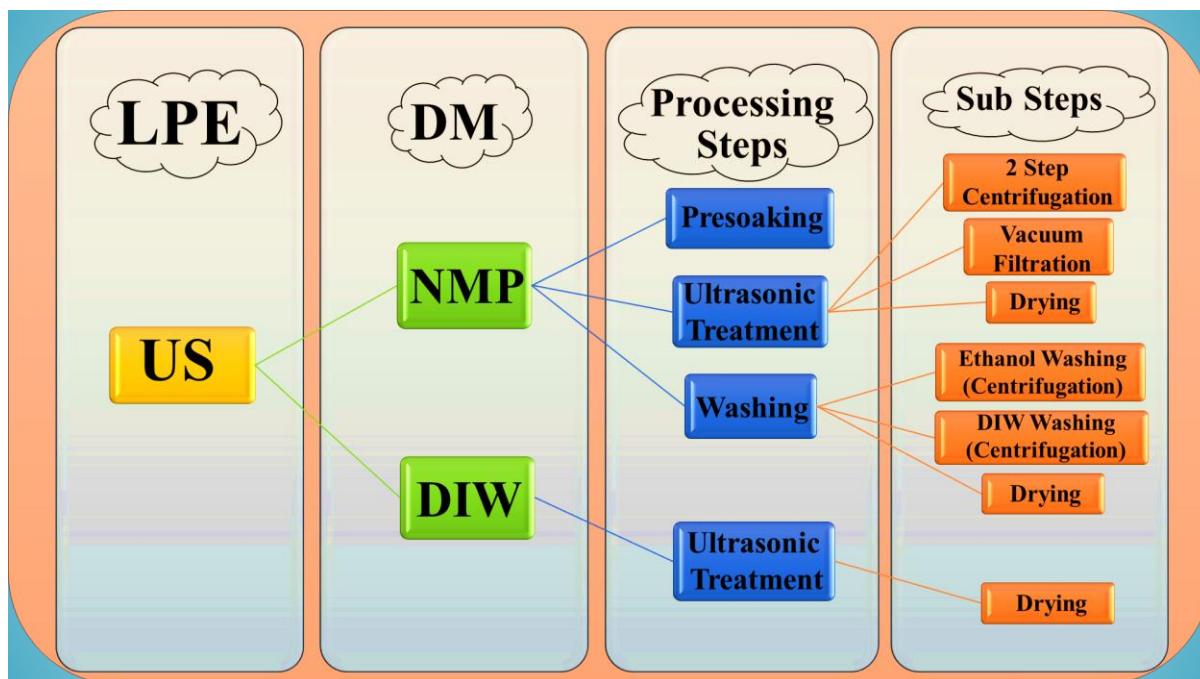
Figure 5.10: Comparative flow chart of liquid phase exfoliation in NMP and DI Water *as Dispersive Medium*

5.6   Effect of Ultrasonic Parameters

5.6.1   *Input power*

In Experiment 2a, the duration for the ultrasonic treatment was set at 6 hours, but all other factors remained the same as previously described. The input power of the ultrasonication was modified, with adjustments made to three distinct levels: 390 W (60% of the original power), 520 W (80% of the original power), and 650 W (100% of the original power). The samples were designated as US-P1, US-P2, and US-P3, corresponding to power outputs of 390 W, 520 W, and 650 W, respectively. Equation 1 provides the expression for the energy density of acoustic waves [147].

$$Energy \; Density \; = \frac{Power \; (W) \times Time \; (S)}{Volume \; (L)} \quad JL^{-1} \qquad \ldots\ldots\ldots 1$$

Therefore, the energy densities (ED) associated with the respective power outputs were determined to be 84.24 kJ.mL^{-1} for 390 W, 112.32 kJ.mL^{-1} for 520 W, and 140.40 kJ.mL^{-1} for 650 W.
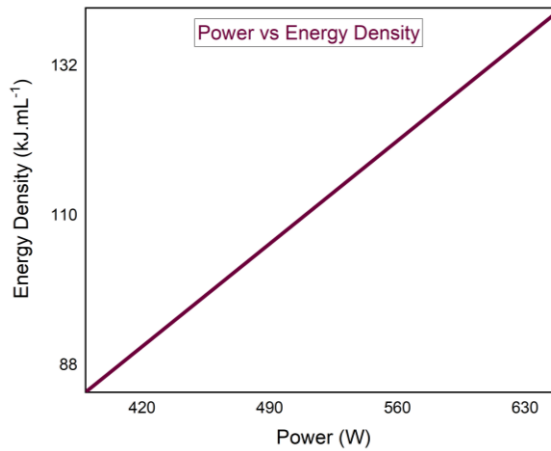
Figure 5.11: The graph illustrating the relationship between energy density and input power.

The graphical representation depicted in Figure 5.11 illustrates a straight proportionality between the energy density (ED) and, therefore, the inertial cavitation dosage (ICD) with respect to the input power. The ED given to the DM for the exfoliation of 2D TiB$_2$ can be enhanced in the cavitation zone of ultrasonication by augmenting the input power.

5.6.2   Treatment Time

In Experiment 2b, we investigated the impact of the duration of ultrasonic treatment. This was achieved by keeping all other parameters constant and setting the input power at a fixed value of 650 W.

The adjustment of US time was executed by a three-step process, namely, a 6-hour shift denoted as US-T1, followed by a 7-hour shift referred to as US-T2, and finally an 8-hour shift designated as US-T3.

The energy density (ED) values obtained for 6 hours, 7 hours, and 8 hours of ultrasonication were 140.40 kJ.mL^{-1}, 163.80 kJ.mL^{-1}, and 187.20 kJ.mL^{-1}, respectively. The data presented in Figure 5.12 demonstrates that the duration of ultrasonication in the treatment has a corresponding impact on the energy density (ED) given to the system by the Ultrasonic Transducer (UST). Consequently, the inertial cavitation dosage (ICD) exhibits a direct relationship with the interval of ultrasonication.
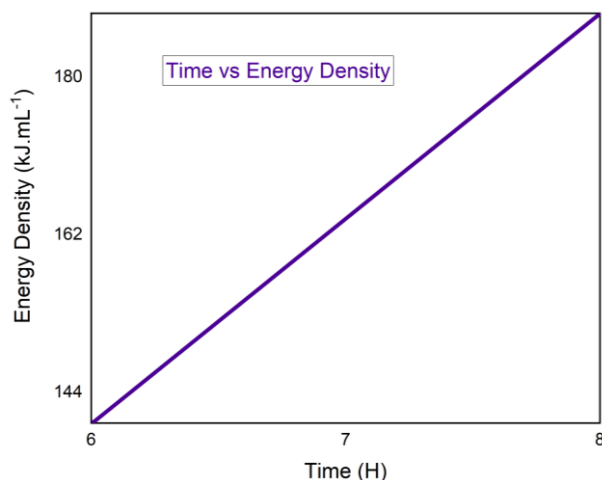
Figure 5.12: The graph illustrating the relationship between energy density and treatment time.

5.7   Comparative XRD Pattern of US-N1 and US-P3

The X-ray diffraction (XRD) patterns presented in Figures 5.3 and 5.5 demonstrate a comparison between US-N1 and US-P3. These patterns indicate that the 2D TiB$_2$ synthesized using liquid phase exfoliation (LPE) in N-methyl-2-pyrrolidone (NMP) contains impurities or NMP molecules that are confined within the layers of the material. The intensities of the peaks exhibited little alterations, accompanied by a limited shift,

indicating a rather low level of exfoliation. Furthermore, the alignment of the sheets was not accurately maintained along the designated plane.

The presence of contaminants in the LPE process of 2D TiB$_2$ necessitates additional processing and washing steps to get pure 2D TiB$_2$, resulting in increased costs. In contrast, the sheets produced using DIW exhibit no impurities or flaws. Furthermore, in the context of DIW, notable changes in the magnitudes of distinct peaks were seen, accompanied by substantial peak displacement, and widening. These observations suggest a high level of exfoliation.

The sheets were aligned appropriately along the (001) crystallographic plane. Therefore, the Liquid Phase Exfoliation (LPE) in Deionized water (DIW) resulted in the production of sheets that were characterized by their purity, cleanliness, and excellent quality. These sheets also exhibited increased lateral dimensions.

5.8   Comparative XRD Pattern of US-N2 and US-T1

The X-ray diffraction (XRD) patterns of US-N2 and US-T1 are presented in Figure 5.3 and 5.8 for comparison. The analysis of the spectra indicated the persistence of residual NMP or contaminants during the washing process, suggesting that additional measures such as heating, or calcination were necessary to achieve the synthesis of pure 2D TiB$_2$.

A notable phenomenon of peak broadening was observed, suggesting the presence of smaller sheets characterized by a wide range of lateral dimensions. In contrast, the Liquid Phase Exfoliation (LPE) technique employed by DIW resulted in the production of highly purified two-dimensional titanium diboride (TiB$_2$) without requiring any additional processing steps. The sheets that are formed have a limited range of increased lateral dimensions. Therefore, the Liquid Phase Exfoliation (LPE) technique in the DIW process offers advantages such as ease of use, cost-effectiveness, time efficiency, and the production of high-quality sheets that are free from flaws or impurities.

Notably, these benefits are achieved without the need for additives, surfactants, or additional ions [83, 84]. The effectiveness of the exfoliation was heavily reliant on the

cavitation process. Therefore, the utilization of Liquid Phase Exfoliation (LPE) using deionized water (DIW) as dispersive medium offers an environmentally friendly approach for the efficient and cost-effective fabrication of two-dimensional titanium diboride (2D TiB_2) on a large scale [90, 104]. The comparison of the sheets that were created is presented in Table 5.1.

Table 5.1: The comparison of the properties of produced sheets of 2D TiB_2 in NMP and

DIW (as DM)

DM	Impurity	Lateral dimension	Defects	Processing Time
NMP	Present	Smaller	Can be present	Long
DIW	Not present	Larger	No defects	Less

5.9 Comparison of Ultrasonic Treatment Parameters

5.9.1 Comparison of Input Power

The X-ray diffraction (XRD) pattern depicted in Figure 5.5 illustrates the comparison of the resulting sheets under varying input powers. It is observed that when the power is increased, the intensities of the distinct peaks undergo alterations, accompanied by an increase in peak shift and widening. The alignment of sheets along the (001) crystallographic plane is also enhanced.

The comparison of X-ray diffraction (XRD) patterns (Figure 5.5), scanning electron microscopy (SEM) images (Figure 5.4), and atomic force microscopy (AFM) images (Figure 5.6) of US-P1, US-P2, and US-P3 reveals the presence of significant semi-exfoliated TiB_2 sheets when subjected to an energy density of 84.24 kJ/mL. The sheets in question have bigger dimensions and were composed of many layers of material.

57

The augmentation of energy density from 84.24 kJ/mL to 112.32 kJ/mL, and subsequently to 140.40 kJ/mL, resulted in a rise in the intensity of the cavitation field, hence leading to an increase in the ICD. With an energy density of 140.40 kJ/mL, the ICD exhibited significant strength, resulting in the application of a substantial force to the layers of BTB, causing their exfoliation into a two-dimensional TiB_2 material.

The lateral dimensions exhibit a reduction from 10 μm to 5 μm. The thickness of the layer exhibits a substantial drop, transitioning from a value over 100 nanometers to around 35 nanometers. There is a substantial rise in the ratio of lateral dimensions to layer thickness, ranging from 34 to 145. This observation demonstrates that the reduction in layer thickness and the enhancement of exfoliation are directly proportional to the rise in power and concentration of 2D TiB_2 dispersion. Table 5.2 illustrates the impact of power on the resulting sheet.

Table 5.2: The comparison of the properties of produced sheets of in Samples US-P1, US-P2 and US-P3

Input Power (W)	Energy Density (kJ/mL)	Lateral Dimension (μm)	Layer Thickness (nm)	Lateral dimensions to thickness Ratio	Defect	Impurity	Time (h)
390	84.24	10	> 100	34	No	No	6
520	112.32	6	68	88	No	No	6
650	140.40	5	35	145	No	No	6

5.9.2   Comparison of Treatment Time

The impact of varying the period of treatment in the Ultrasonic treatment has been demonstrated by the comparative X-ray diffraction (XRD) patterns seen in Figure 5.8. The

X-ray diffraction (XRD) patterns exhibit a notable displacement of peaks and alterations in intensities, which are consistent with the formation of two-dimensional titanium diboride (2D TiB$_2$) across all time intervals. These observations indicate a substantial degree of exfoliation and precise alignment along the (001) crystallographic plane.

However, the phenomenon of peak broadening is shown to be more pronounced when the duration of ultrasonic (US) treatment is prolonged. This effect is indicative of the fracturing or fracture of lateral dimensions as well as the thickness of the layers. The phenomenon becomes more pronounced when the length of the event or condition is extended.

The analysis of X-ray diffraction (XRD) patterns (refer to figure 5.8), scanning electron microscopy (SEM) pictures (refer to figure 5.7), and atomic force microscopy (AFM) images (refer to figure 5.9) for samples US-T1, US-T2, and US-T3 reveals that, when subjected to an energy density of 140.4 kJ/mL, significant quantities of well-separated TiB$_2$ sheets were seen. The dimensions of these sheets were comparatively bigger laterally, and their layer count was below 100.

The enhancement of the energy density from 140.4 kJ/mL to 163.8 kJ/mL and subsequently to 187.2 kJ/mL resulted in an augmented impact of ICD, therefore leading to an extended duration of the cavitation field's intensity.

With an energy density of 187.2 kJ/mL, the ICD exhibited significant strength, delivering a substantial amount of force over an extended period to the layers of BTB. This resulted in the exfoliation of the layers into a two-dimensional TiB$_2$ structure, accompanied by sheet breakage and reduction in lateral dimensions.

The reduction in layer thickness from 34 nm to 21 nm was seen when the treatment duration was increased from 6 hours to 8 hours. Nevertheless, there was a notable drop in the lateral dimensions, ranging from 5 µm to 1 µm.

Additionally, the ratio of lateral dimensions to layer thickness exhibited a considerable shift, decreasing from 148 to 47. Defects were also introduced to a certain

degree over an extended period. Table 5.3 displays the impact of the duration of US treatment on the resulting sheet.

Table 5.3: The comparison of the properties of produced sheets of in Samples US-P1, US-P2 and US-P3

Duration (h)	Energy Density (kJ/mL)	Lateral Dimension (µm)	Layer Thickness (nm)	Lateral dimensions to thickness Ratio	Defect	Impurity	Input Power (W)
6	140.40	5	34	148	No	No	650
7	163.80	3.5	31	110	Not Significant	No	650
8	187.20	< 1	21	47	Up to some extent	No	650

CHAPTER 6: MECHANISMS

6.1   Mechanism of Ultrasonic Treatment

This study aimed to examine the impact of liquid phase exfoliation (LPE) on 2D titanium diboride (TiB_2) sheets by dividing the operations conducted in the ultrasonication using various inertial cavitation dosages (ICDs) into two distinct segments.

Initially, the phenomenon of cavitation was detected by the manipulation of the input variable, while ensuring that the length of the treatment remained constant at 6 hours. In the subsequent section, a consistent power level of 650 W was upheld, while the occurrence of cavitation was investigated by alterations in the period of the treatment. The main aim of our work was to get a deeper understanding of the key elements that contribute to the formation of the final structure of few-layered 2D TiB_2 (FLTB) sheets when they are dispersed in water, with a particular focus on cavitation.

The basic mechanism behind liquid phase exfoliation (LPE) via cavitation, like other solvent-based techniques in the ultrasonication treatment, is the implosion of microscale bubbles experiencing vigorous oscillations [190]. The bubbles exhibit a considerable quantity of potential energy. Following a catastrophic collapse event, a rapid discharge of energy occurs, leading to the formation of liquid micro-jets characterized by high velocities within the range of 100 to 500 m/s [191]. The high-pressure shock waves generated can reach magnitudes of up to 1 gigapascal (GPa) [192, 193].

Additionally, localized zones with heightened temperatures of around 10^4 Kelvin (K) are also formed [194, 195]. The process undergoes several iterations within a unitary second and is widely acknowledged as the principal mechanism responsible for the exfoliation of two-dimensional (2D) materials. The dimensions and lifespan of cavitation bubbles can exhibit variability, displaying both individual and collective characteristics, such as forming a cluster of bubbles [196]. The collective conduct shown by individuals can exert a significant influence on the dynamics of bubbles. Moreover, the dynamics of

cavitation bubbles can exhibit either a constant or transient nature, contingent upon the specific attributes of the acoustic pressure field to which they are exposed [197].

These events are significant in controlling the cavitation process and have the capacity to influence the mechanism of BTB exfoliation. Due to the intrinsic unpredictability and fluidity of the surrounding environment, it is impracticable to exercise direct governance over the individual conduct of bubbles. Therefore, modifications to the characteristics of the ultrasonic treatment are implemented through the examination of the collective behavior of bubble clouds and the subsequent pressure waves. The monitoring approach facilitates the identification of required adjustments to the parameters of the ultrasonication [104].

6.2   Mechanism of Input Power

The correlation shown in equation 3 illustrates the connection between the driving frequency (f) and the vibration amplitude (A), which is contingent upon the input power. This relationship plays a crucial role in defining the acoustic power (W), which subsequently impacts the average size of the bubbles. Likewise, the acoustic power (W) exerts an influence on the concentration of bubbles. The occurrence of cavitation relies on the acoustic power (AP), whereas the Intensity magnitude of cavitation (CI) is directly correlated with the energy produced by the bubbles [104].

$$Acoustic\ Power \approx A^2 \times f^2 \qquad\qquad \text{………. 3}$$

The findings of this study indicate that the initial application of AP was insufficient in effectively exfoliating the layers of TiB_2. The cavitation intensity in the cavitation zone was shown to exhibit a significant lack of strength. Consequently, the ultrasonic treatment had a reduced quantity of bubbles, which were characterized by greater dimensions, namely in size [190]. The pressure resulting from cavitation and its distribution across the volume of the CZ were insufficient to achieve a significant exfoliating impact through the cavitation induced by these bubbles [197].

The modest exfoliation rate observed can be attributed to the combined influence of the cavitation bubbles' size, activity, and concentration [196]. Consequently, in conditions of low acoustic power (AP), substantial areas of partially exfoliated titanium diboride (TiB$_2$) were seen. The sheets in question have bigger dimensions and were composed of many layers of material. The augmentation of the acoustic power (AP) resulted in an amplification of the intensity of the cavitation field.

At elevated acoustic power (AP), the cavitation field (CF) exhibited considerable strength, resulting in a substantial application of force onto the layers of Bulk TiB$_2$ (BTB), causing their exfoliation into two-dimensional titanium diboride (2D TiB$_2$) [83]. This observation demonstrates that an increase in power leads to a reduction in layer thickness, whereas an increase in concentration results in a higher degree of exfoliation.

6.3   Mechanism of Treatment Time

The determination of the inertial cavitation dose (ICD) is contingent upon the energy density (ED) shown by the bubbles. This energy density is influenced by two key elements: the treatment time (t) and the input power (W). These factors play a crucial role in regulating the quantity of energy managed to be provided to the BTB layers. The equation for determining energy density is provided in Equation 3 [147].

$$Energy\ Density\ = \frac{Power\ (W) \times Time\ (S)}{Volume\ (L)} \quad JL^{-1} \quad \dots\dots 1$$

Therefore, the cavitation intensity was deemed sufficient for reducing treatment time, as the bubbles exhibited significant size, concentration, and activity, resulting in substantial pressure generation within the cavitation zone [198]. The pressure and energy density exhibited a distribution that predominantly resulted in the application of shear forces, which primarily served to induce separation between the layers without causing their rupture. The cavitation zone was adequately characterized by the given ICD.

The use of expanded treatment in the ultrasonication resulted in an extended duration of pressure exerted by the bubbles, leading to the generation of smaller bubbles

with greater quantities over an extended period. The severity of the cavitation field caused the sheets to shatter, in addition to their exfoliation [101, 199].

6.4   Mechanism of Treatment Time

The consideration of frequency is also pertinent as the acoustic cavitation's acoustic power (AP) exerted on the system is primarily influenced by the amplitude of the cavitation field, (which is regulated by the input power) (A) and the frequency (f) of said field. Equation 4 presents the mathematical representation of the association between the AP (acoustic power) delivered to the DM (dispersive medium) during the ultrasonication (US).

$$Caviation\ Intensity\ (input\ power\ of\ acoustic\ field) = 2\pi\rho c \times f^2 A^2 \times \frac{\pi\varphi^2}{4} \quad ......4$$

In this context, ρ represents the density of the dispersive media, denoted as DIW. The variable c denotes the velocity of ultrasound waves in the dispersive medium. f represents the input frequency, while A signifies the amplitude of the ultrasonic waves generated by the sonotrode. The amplitude A of the sonotrode transducer is influenced by the input power. The impact of both amplitude and frequency on acoustic input power is equivalent, therefore implying that the influence of frequency on the extent of exfoliation should mirror that of the input power supplied to the sonotrode.

The following considerations pertaining to frequency are derived from equation 4 and observed investigations conducted on the influence of input power (amplitude). These claims are substantiated by existing scholarly literature, but our study did not specifically investigate them.

The exfoliation process conducted at lower frequencies shows reduced effectiveness in comparison to the other investigated regimes in the ultrasonic frequencies. Samples obtained at higher frequencies will have a more pronounced level of exfoliation. At elevated frequencies, the 2D sheets will exhibit a significantly reduced layer thickness, resulting in a limited number of material layers within them. The ultrasonic (US) arrangement with the greatest frequency will yield the observation of the thinnest sheets [104].

As a result, with increasing frequency, the thickness of the 2D sheets decreases. Furthermore, it is important to acknowledge that the density of two-dimensional sheets, specifically the quantity of exfoliated sheets inside a solution, in a DIW (deionized water) solution, plays a pivotal role in future applications and the production of goods on a big scale. The ultrasonic probe transducer (UST), also known as the sonotrode, when submerged in deionized water (DIW) and operated at a higher frequency, can generate solution sheets consisting of a few layers of two-dimensional (2D) material with a very high concentration [200].

6.5   Mechanism of Geometrical Configuration

The dose of inertial cavitation (ICD) varies across various use zones, contingent upon the characteristics of the ultrasound (US) as determined by the ultrasound transducer (UST). Equation 5 provides the expression for the ratio between the volume of the CZ (v_{6mm}) and the treated volume, denoted as V, in the context of the given scenario [196]. This ratio characterizes the allocation of energy in the context of cavitation occurring within a the volume of the vessel [104].

$$\frac{v_{6mm}}{V} = 0.0034 \qquad \qquad ……….5$$

To understand the importance of the configuration geometry of the ultrasonic setup (US) within the framework of our investigation, we may conduct a comparison of the X-ray diffraction (XRD) plots depicted in Figure 5.8.

These plots pertain to the samples labeled as US-T1, US-T2, and US-T3. An observable phenomenon of considerable widening was seen upon extending the duration of our treatment. This observation demonstrates the occurrence of lateral dimension fractures. The results obtained from the SEM analysis depicted in Figures 5.7 exhibit the same findings as shown by XRD. The primary factor contributing to the fracture of the sheets was the diameter or dimensions of the sonotrode.

By keeping a constant frequency of around 25 kHz and power output of 650 W, we ensured a consistent level of cavitation intensity while running. Nevertheless, the

augmentation of treatment duration resulted in an amplification of the cavitation field or intensity, leading to an elevation in energy density. Consequently, the dispersive medium received a higher level of energy, as delivered by the sonotrode [101, 199].

The ultrasonic field displayed a higher level of variability for a 6-mm sonotrode. The phenomenon described involved the emission of acoustic energy in proximity to the sonotrode tip, leading to the creation of a localized region of intense cavitation, commonly referred to as the highly concentrated cavitation zone (CZ) [104]. The cavitation zone (CZ) exhibited a downward expansion in a conical shape and underwent significant attenuation because of the shielding effect, as shown in the study conducted by the researchers [196].

As a result, certain areas of the vessel, located at a greater distance from the tip, exhibited limited effect of ultrasonication and were referred to as "dead zones" [104]. The impact of secondary acoustic fluxes on the sonotrode with reduced diameter is minimal and does not significantly alter the observed effect [201]. Therefore, the utilization of the 6-mm ST led to the formation of a highly concentrated CZ.

The cavitation zone (CZ) had a diameter approximately 1.5 times larger than that of the ST [145]. This observation indicates a disparity of 9 mm and 60 mm between the diameter of the active CZ and the vessel size, as seen in Figure 3.2.

Therefore, it can be demonstrated that the 6-mm ST efficiently generated a region of cavitation that included just a fraction of the treated volume, while the area furthest from the tip of the sonotrode was characterized as the "dead zone". As a result of the non-uniform distribution of the CF, the ED applied a treatment to the sheets that significantly fractured the lateral dimension while also decreasing the thickness of each layer. The impact was further intensified due to the extended duration of the treatment.

By employing a sonotrode tip of larger diameter, the uniformity of the ultrasonic (US) field distribution inside the solution volume will be enhanced. This effect is particularly pronounced when the diameters of the sonotrode tip (ST) and the vessel are in proximity, resulting in a more homogeneous cavitation zone (CZ). The implementation of a homogeneous cavitation treatment is expected to result in a more uniform dispersion of

a limited number of two-dimensional titanium diboride (FLTB) sheets, both in terms of their size and thickness.

This contrasts with the setup featuring a concentrated CZ. Therefore, the smaller ST, although having an equivalent input power, demonstrated a higher level of cavitation concentration inside a reduced volume. As a result, this phenomenon resulted in a higher frequency of opportunities for the occurrence of defective structures in the ultimate 2D TiB_2 sheets.

6.6   Mechanism of Sonoexfoliation

The complicated relationship between the processes underlying the process of Sonoexfoliation, specifically ultrasonic exfoliation, of two-dimensional TiB_2 sheets can be attributed to the well-established phenomenon of cavitation. The size, distribution, number, collapse, and spatial distribution of bubbles within a vessel are important features that may be modified by several parameters such as frequency, power (amplitude), treatment duration, and configuration geometry of the experimental setup [202, 203].

Figure 6.1 displays the schematic depiction of the Liquid Phase exfoliation (LPE) process for synthesizing two-dimensional titanium diboride (TiB_2) using ultrasonication (US) treatment of the BTB.

There were no discernible differences seen in the structural defect of the generated 2D TiB_2 when modifying the power (amplitude) and duration of the ultrasonic treatment. This is evident from the scanning electron microscopy (SEM) pictures. The findings from the SEM, XRD, and AFM analyses elucidated the correlation between the thickness of the sheets and the driving power and treatment duration. The study revealed that an increase in power or treatment duration resulted in a decrease in thickness and varying levels of cavitation intensity in the few layer 2D TiB_2 sheets.

The Minnaert equation offers a theoretical estimation of the linear resonance size (LRS) of bubbles produced by cavitation [204, 205]. The collapse of the bubble at the LRS is subject to influence from both the acoustic frequency and power. At a frequency of

around 25 kHz and operating at 100% power, the linear response size (LRS) of the bubble in water was estimated to be approximately 140 μm [206].
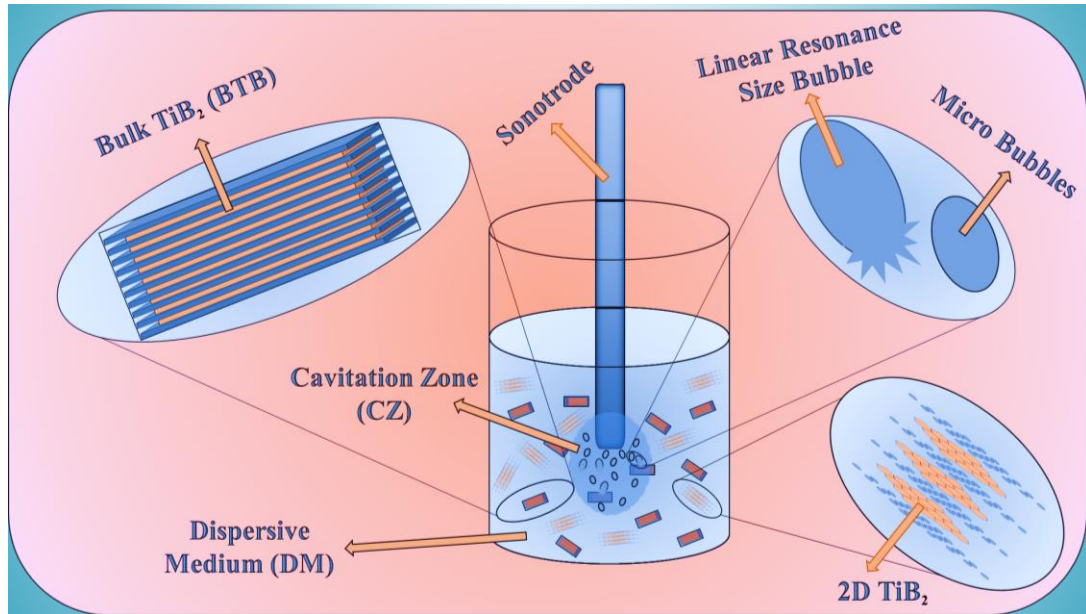
Figure 6.1: Schematic representation of the Liquid Phase Exfoliation of 2D TiB$_2$.

The Minnaert equation offers a theoretical estimation of the linear resonance size (LRS) of bubbles produced by cavitation [204, 205]. The collapse of the bubble at the LRS is subject to influence from both the acoustic frequency and power. At a frequency of around 25 kHz and operating at 100% power, the linear response size (LRS) of the bubble in water was estimated to be approximately 140 μm [206].

Bubbles within a particular range of resonance size tend to collapse under the influence of proper linear response size (LRS), leading to the creation of liquid micro-jets (LMJ) at the nanoscale [207]. According to previous experimental findings, it has been observed that the LMJ (liquid micro-jets) tip measures approximately one-tenth of the maximum or resonant bubble radius [191].

Additionally, the occurrence of cavitation bubbles (CB) leads to a series of chain reactions and multiplication, resulting in the formation of smaller bubbles with decreased dimensions [208, 209]. These smaller bubbles are widely known as nanobubbles [210].

The nanobubbles produced during the chain reaction display a size more than 30 nm [210], which surpasses the interlayer spacing of TiB_2. Nevertheless, these entities continue to be vulnerable to stimulation caused by shock waves or the occurrence of a 25 kHz incident frequency. This susceptibility results in the emergence of intense oscillations and the production of diverse vibrating patterns referred to as "Faraday or surface waves" (SW) [211].

The occurrence of resonance in the MHz frequency range leads to the emergence of unstable, strongly non-linear, chaotic, and dynamic structures [212]. The bubble pressures can attain magnitudes of several hundred kilopascals (kPa) [211, 212], which is adequate to induce the delamination of the TiB_2 layers, as evidenced by previous investigations on other two-dimensional (2D) materials [213].

Based on the available evidence, it can be deduced that the utilization of high-frequency or high-power ultrasound treatment, with a diameter similar to that of the vessel, resulted in the emission of relatively mild jets. This occurrence is likely attributed to the vigorous contraction or implosion action.

This particular treatment was considered to be more suitable for the goal of exfoliation because of its ability to generate smaller-sized CB formations. As the frequency of the phenomenon increased, there was a corresponding drop in both the size of the collapsing CB and the time of the collapse, as shown by previous studies [214].

On the other hand, employing a ST operating at a reduced frequency or power level leads to the development of larger cavitation bubbles (CBs) that demonstrate more vigorous collapse. This phenomenon has the potential to increase the dispersion of sheets, resulting in a higher concentration of FLTB sheets in the solution. Nevertheless, it is crucial to acknowledge that this methodology also produces a significant number of diminutive cavitation bubbles.

The utilization of micrometer-sized cavitation bubbles (CB) has promised to induce fractures in the lateral dimensions of sheets, specifically in a direction that is perpendicular to the planes of titanium diboride (TiB_2). On the contrary, it is hypothesized that smaller

bubbles have the capacity to subtly increase the interlayer spacing inside the TiB_2 layers [104].

The combination of the US bath sonicator (BUS) and US Probe Sonicator (PUS) approaches shows promise for industrial scale-up in producing cavitation. These results are consistent with previous research, in which the researchers employed a hybrid approach using a 30 kHz broadband ultrasonic system (BUS) and a 20 kHz power ultrasonic sonotrode (PUS), together with surfactants and chemical exfoliation agents [83].

Sonochemistry provides a supplementary mechanism for the process of cavitation-induced exfoliation in aquatic settings. The primary cause of the layer-by-layer exfoliation of 2D sheets in DIW can be attributed to a sonochemical reaction involving the free radicals produced by the collapse of CB, as shown in a previous work [94].

The experimental procedure in the ultrasonic treatment involved subjecting the samples to two different temperatures, namely 40°C and 60°C, using a 40-kHz ultrasonic bath for a duration of 60 hours.

The researchers reached the conclusion that the observed phenomena of exfoliation were only caused by the presence of cavitation, which was exclusively obtained at the elevated temperature of 60 °C. This research primarily concentrates on the domain of chemistry, with less emphasis placed on the complete exploration of US features and cavitation [94].

Based on the results obtained from our experimental investigation, it can be inferred that the exfoliation of 2D TiB_2 during ultrasonic cavitation treatment is attributed to physico-mechanical mechanisms. The phenomenon of exfoliation, which can be investigated through the utilization of high-speed photography techniques, reveals that the splitting of TiB_2 sheets is a result of the oscillation and collapse of the cavitation bubbles (CB), as demonstrated in a prior work [213].

The present study offers a comprehensive depiction of the mechanism via which CB, emanating from the ST tip, induces the fragmentation of 2D sheets. Following this,

the cavitation bubbles gradually remove the layers by infiltrating the crevices between the layers within the structure [213].

CHAPTER 7:   CONCLUSIONS AND FUTURE RECOMMENDATION

7.1   Conclusion

This study aimed to examine the process of exfoliation for a newly discovered two-dimensional material, specifically 2D TiB_2. Initially, an examination was conducted on the ramifications of dispersive media. The 6-hour exfoliation process at 650 W power utilized NMP and DIW, employing the identical vessel and sonotrode arrangement.

Highly pure two-dimensional (2D) sheets of titanium diboride (TiB_2) were successfully produced using deionized (DI) water, resulting in the absence of impurities or flaws. The removal of NMP from 2D sheets of TiB_2 was a challenging task. Moreover, the exfoliation technique employed in DIW demonstrates cost-effectiveness, scalability, and efficiency due to its streamlined single-step procedure. Next, the impact of several ultrasonic liquid phase exfoliation parameters, namely power, treatment duration, and configuration geometry, on the properties of a few-layered two-dimensional titanium diboride (FLTB) generated in deionized water (DIW) without the use of chemical surfactants was investigated.

The experiment consisted of two phases, wherein a vessel with a diameter of 60 mm was utilized. The amount of the water-BTB solution employed in the experiment was 100 ml, and it was kept at a temperature of 40 °C. In the initial phase, the treatment duration was set at 6 hours while the power was modified. In the subsequent phase, the treatment duration was altered while keeping the power constant at 650 W.

The attainment of superior quality, few layers TiB_2 (FLTB) was ascribed to the existence of a diverse dispersion of cavitation occurrences inside the processed volume, aided by primary and secondary sonic flows. The experimental results demonstrated that the desired outcomes were obtained by manipulating the lateral dimensions and thickness of a two-dimensional titanium diboride (TiB_2) material.

Specifically, the best outcomes were reached by increasing the lateral dimensions to around 5 μm and reducing the thickness to roughly 35 nm. This was accomplished by

employing a sonotrode with a considerable size of 6 mm, operating at a frequency of 25 kHz, and subjecting the material to ultrasonication for a duration of 6 hours using a power of 650 W.

Based on the most recent research findings in this field, it can be deduced that our results are consistent with the most favorable outcomes observed in the context of 2D TiB_2 Sonoexfoliation conducted in aquatic settings. The potential practical use of liquid phase exfoliation (LPE) may be observed through the employment of a high-frequency sonication strategy, which involves varying powers and treatment time durations.

This approach demonstrates the ability to achieve LPE without the inclusion of harmful chemicals. Increasing the input power or treatment duration results in a reduction in the average thickness of the resultant FLTB and improves the efficiency of cavitation-induced liquid phase exfoliation (LPE). The prolonged duration of treatment and its impact on the dimensions of the probe also result in the breakdown of lateral dimensions. The utilization of an optimal treatment duration has the potential to yield significant improvements in the production of big, high-quality two-dimensional titanium diboride (TiB_2) materials, while simultaneously reducing their thickness.

To get bigger sheets with considerably increased lateral dimensions and a decreased thickness over a few layers, it is advisable to ensure that the diameter of the probe is equivalent to the size or diameter of the vessel. The exfoliation of 2D TiB_2 in water is hypothesized to occur by the mechanical action of small active cavitation bubbles. These bubbles are believed to aid in the dispersion and exfoliation of a limited number of stacked 2D TiB_2 sheets. The 2D TiB_2 sheets exhibit exceptional quality and purity, rendering them suitable for a range of applications such as energy storage, water splitting, and photocatalysis.

7.2   Future Recommendations

There is a requirement for enhancement in several facets of the generated two-dimensional titanium diboride (2D TiB_2), specifically in terms of thickness uniformity and yield. These improvements are imperative to enable the practical large-scale

production of freestanding few layers titanium boride (FLTB) sheets. Future research endeavors will prioritize the amalgamation of multiple ultrasonic sources with varying frequency ranges, power levels, geometrical configurations, sonotrode sizes and configurations, treatment durations, and setups.

The objective is to generate larger 2D TiB_2 sheets with consistent lateral dimensions, thickness, and a significantly high yield suitable for industrial or practical large-scale manufacturing purposes. Utilizing in-situ observations for the examination of cavitation-induced exfoliation holds the potential to enhance comprehension of the fundamental mechanisms governing this event. Further investigation is required to explore the possible uses of two-dimensional titanium diboride (2D TiB_2).

REFERENCES

[1]   G. A. Naikoo *et al.*, "2D materials, synthesis, characterization and toxicity: A critical review," *Chemico-Biological Interactions,* p. 110081, 2022.

[2]   Y. Chen *et al.*, "Two-dimensional metal nanomaterials: synthesis, properties, and applications," *Chemical reviews,* vol. 118, no. 13, pp. 6409-6455, 2018.

[3]   C. Tan *et al.*, "Recent Advances in Ultrathin Two-Dimensional Nanomaterials," *Chem Rev,* vol. 117, no. 9, pp. 6225-6331, May 10 2017.

[4]   C. Huo, Z. Yan, X. Song, and H. Zeng, "2D materials via liquid exfoliation: a review on fabrication and applications," *Science bulletin,* vol. 60, no. 23, pp. 1994-2008, 2015.

[5]   H. Zhang, "Ultrathin two-dimensional nanomaterials," *ACS nano,* vol. 9, no. 10, pp. 9451-9469, 2015.

[6]   B. Mendoza-Sánchez and Y. Gogotsi, "Synthesis of two-dimensional materials for capacitive energy storage," *Advanced Materials,* vol. 28, no. 29, pp. 6104-6135, 2016.

[7]   C. Tan, Z. Liu, W. Huang, and H. Zhang, "Non-volatile resistive memory devices based on solution-processed ultrathin two-dimensional nanomaterials," *Chemical society reviews,* vol. 44, no. 9, pp. 2615-2628, 2015.

[8]   D. Deng, K. Novoselov, Q. Fu, N. Zheng, Z. Tian, and X. Bao, "Catalysis with two-dimensional materials and their heterostructures," *Nature nanotechnology,* vol. 11, no. 3, pp. 218-230, 2016.

[9]   F. Bonaccorso *et al.*, "Graphene, related two-dimensional crystals, and hybrid systems for energy conversion and storage," *Science,* vol. 347, no. 6217, p. 1246501, 2015.

[10]   G. Fiori *et al.*, "Electronics based on two-dimensional materials," *Nature nanotechnology,* vol. 9, no. 10, pp. 768-779, 2014.

[11]   M. Chhowalla, D. Jena, and H. Zhang, "Two-dimensional semiconductors for transistors," *Nature Reviews Materials,* vol. 1, no. 11, pp. 1-15, 2016.

[12]   Y. Chen *et al.*, "Two-Dimensional Metal Nanomaterials: Synthesis, Properties, and Applications," *Chem Rev,* vol. 118, no. 13, pp. 6409-6455, Jul 11 2018.

[13]   X. Cai, Y. Luo, B. Liu, and H. M. Cheng, "Preparation of 2D material dispersions and their applications," *Chem Soc Rev,* vol. 47, no. 16, pp. 6224-6266, Aug 13 2018.

[14]   Y. Sun, S. Gao, and Y. Xie, "Atomically-thick two-dimensional crystals: electronic structure regulation and energy device construction," *Chemical Society Reviews,* vol. 43, no. 2, pp. 530-546, 2014.

[15]   X. Cai, Y. Luo, B. Liu, and H.-M. Cheng, "Preparation of 2D material dispersions and their applications," *Chemical Society Reviews,* vol. 47, no. 16, pp. 6224-6266, 2018.

[16]   G. Rinaldi, "Nanoscience and technology: a collection of reviews from nature journals," *Assembly Automation,* vol. 30, no. 2, 2010.

[17]   X. Xiao, H. Wang, P. Urbankowski, and Y. Gogotsi, "Topochemical synthesis of 2D materials," *Chemical Society Reviews,* vol. 47, no. 23, pp. 8744-8765, 2018.

[18]   T. H. Le, Y. Oh, H. Kim, and H. Yoon, "Exfoliation of 2D materials for energy and environmental applications," *Chemistry–A European Journal,* vol. 26, no. 29, pp. 6360-6401, 2020.

[19]   J. An *et al.*, "Perspectives of 2D materials for optoelectronic integration," *Advanced Functional Materials,* vol. 32, no. 14, p. 2110119, 2022.

[20]   M. Pumera and A. H. Loo, "Layered transition-metal dichalcogenides (MoS2 and WS2) for sensing and biosensing," *TrAC Trends in Analytical Chemistry,* vol. 61, pp. 49-53, 2014.

[21]   M. Donarelli and L. Ottaviano, "2D materials for gas sensing applications: a review on graphene oxide, MoS2, WS2 and phosphorene," *Sensors,* vol. 18, no. 11, p. 3638, 2018.

[22]   C. Lan, C. Li, J. C. Ho, and Y. Liu, "2D WS2: from vapor phase synthesis to device applications," *Advanced Electronic Materials,* vol. 7, no. 7, p. 2000688, 2021.

[23]   K. S. Novoselov *et al.*, "Electric field effect in atomically thin carbon films," *science,* vol. 306, no. 5696, pp. 666-669, 2004.

[24]   M. S. Stark, K. L. Kuntz, S. J. Martens, and S. C. Warren, "Intercalation of layered materials from bulk to 2D," *Advanced Materials,* vol. 31, no. 27, p. 1808213, 2019.

[25]   G. Yoon, D.-H. Seo, K. Ku, J. Kim, S. Jeon, and K. Kang, "Factors affecting the exfoliation of graphite intercalation compounds for graphene synthesis," *Chemistry of Materials,* vol. 27, no. 6, pp. 2067-2073, 2015.

[26]   A. Yousaf *et al.*, "Exfoliation of quasi-two-dimensional nanosheets of metal diborides," *The Journal of Physical Chemistry C,* vol. 125, no. 12, pp. 6787-6799, 2021.

[27] W. G. Fahrenholtz, G. E. Hilmas, I. G. Talmy, and J. A. Zaykoski, "Refractory diborides of zirconium and hafnium," *Journal of the American Ceramic Society,* vol. 90, no. 5, pp. 1347-1364, 2007.

[28] P. Vajeeston, P. Ravindran, C. Ravi, and R. Asokamani, "Electronic structure, bonding, and ground-state properties of AlB 2-type transition-metal diborides," *Physical Review B,* vol. 63, no. 4, p. 045115, 2001.

[29] X. Xu *et al.*, "The thermodynamic, electronic and elastic properties of the early-transition-metal diborides with AlB2-type structure: A density functional theory study," *Journal of alloys and compounds,* vol. 607, pp. 198-206, 2014.

[30] E. Sani *et al.*, "Titanium diboride ceramics for solar thermal absorbers," *Solar Energy Materials and Solar Cells,* vol. 169, pp. 313-319, 2017.

[31] A. Yousaf *et al.*, "Exfoliation of Quasi-Two-Dimensional Nanosheets of Metal Diborides," *The Journal of Physical Chemistry C,* vol. 125, no. 12, pp. 6787-6799, 2021.

[32] M. Estruga, L. Chen, H. Choi, X. Li, and S. Jin, "Ultrasonic-assisted synthesis of surface-clean TiB2 nanoparticles and their improved dispersion and capture in Al-matrix nanocomposites," *ACS applied materials & interfaces,* vol. 5, no. 17, pp. 8813-8819, 2013.

[33] T. Lundström, "Transition metal borides," in *Boron and Refractory Borides*: Springer, 1977, pp. 351-376.

[34] P. Spoor, J. Maynard, M. Pan, D. Green, J. Hellmann, and T. Tanaka, "Elastic constants and crystal anisotropy of titanium diboride," *Applied physics letters,* vol. 70, no. 15, pp. 1959-1961, 1997.

[35] L. Silvestroni, H.-J. Kleebe, W. G. Fahrenholtz, and J. Watts, "Super-strong materials for temperatures exceeding 2000° C," *Scientific Reports,* vol. 7, no. 1, p. 40730, 2017.

[36] M. M. Opeka, I. G. Talmy, and J. Zaykoski, "Oxidation-based materials selection for 2000 C+ hypersonic aerosurfaces: Theoretical considerations and historical experience," *Journal of materials science,* vol. 39, pp. 5887-5904, 2004.

[37] S. Jayaraman, Y. Yang, D. Y. Kim, G. S. Girolami, and J. R. Abelson, "Hafnium diboride thin films by chemical vapor deposition from a single source precursor," *Journal of Vacuum Science & Technology A,* vol. 23, no. 6, pp. 1619-1625, 2005.

[38] Y. Han, Y. Dai, D. Shu, J. Wang, and B. Sun, "Electronic and bonding properties of TiB2," *Journal of alloys and compounds,* vol. 438, no. 1-2, pp. 327-331, 2007.

[39]   J. Shappirio, J. Finnegan, and R. Lux, "Diboride diffusion barriers in silicon and GaAs technology," *Journal of Vacuum Science & Technology B: Microelectronics Processing and Phenomena,* vol. 4, no. 6, pp. 1409-1415, 1986.

[40]   J. Sung, D. M. Goedde, G. S. Girolami, and J. R. Abelson, "Remote-plasma chemical vapor deposition of conformal ZrB 2 films at low temperature: A promising diffusion barrier for ultralarge scale integrated electronics," *Journal of applied physics,* vol. 91, no. 6, pp. 3904-3911, 2002.

[41]   W. Fahrenholtz and G. Hilmas, "Oxidation of ultra-high temperature transition metal diboride ceramics," *International Materials Reviews,* vol. 57, no. 1, pp. 61-72, 2012.

[42]   C. Sanchez, B. R. Plata, M. M. da Costa, and F. Freire Jr, "Titanium diboride thin films produced by dc-magnetron sputtering: Structural and mechanical properties," *Surface and Coatings Technology,* vol. 205, no. 12, pp. 3698-3702, 2011.

[43]   B. Basu, G. Raju, and A. Suri, "Processing and properties of monolithic TiB2 based materials," *International materials reviews,* vol. 51, no. 6, pp. 352-374, 2006.

[44]   D. Demirskyi, I. Solodkyi, T. Nishimura, and O. O. Vasylkiv, "Fracture and property relationships in the double diboride ceramic composites by spark plasma sintering of TiB2 and NbB2," *Journal of the American Ceramic Society,* vol. 102, no. 7, pp. 4259-4271, 2019.

[45]   J. Justin and A. Jankowiak, "Ultra High Temperature Ceramics: Densification, Properties and Thermal Stability," *Aerospace Lab,* no. 3, pp. p. 1-11, 2011.

[46]   W. G. Fahrenholtz and G. E. Hilmas, "Ultra-high temperature ceramics: Materials for extreme environments," *Scripta materialia,* vol. 129, pp. 94-99, 2017.

[47]   Z. Fu and R. Koc, "Microstructure and mechanical properties of hot pressed submicron TiB2 powders," *Ceramics International,* vol. 44, no. 8, pp. 9995-9999, 2018.

[48]   C. Subramanian, T. C. Murthy, and A. Suri, "Synthesis and consolidation of titanium diboride," *International Journal of Refractory Metals and Hard Materials,* vol. 25, no. 4, pp. 345-350, 2007.

[49]   R. G. Munro, "Material properties of titanium diboride," *Journal of Research of the National institute of standards and Technology,* vol. 105, no. 5, p. 709, 2000.

[50]   M. Alsawat, T. Altalhi, N. Alotaibi, and Z. Zaki, "Titanium carbide–Titanium boride composites by self propagating high temperature synthesis approach: Influence of zirconia additives on the mechanical properties," *Results in Physics,* vol. 13, p. 102292, 2019.

[51] W. Dai, X. Gao, X. Li, and Q. Wang, "Influence of carbon incorporation on microstructure and properties of titanium diboride coatings deposited by combining ion beam with magnetron sputtering," *Ceramics International,* vol. 45, no. 17, pp. 22498-22505, 2019.

[52] B. Derin, K. Kurtoglu, F. C. Sahin, and O. Yucel, "Thermochemical modeling and experimental studies on the formation of TiB2 through carbothermic synthesis from TiO2 and B2O3 or B4C," *Ceramics International,* vol. 43, no. 14, pp. 10975-10982, 2017.

[53] T. Ma, P. Zhu, and X. Yu, "Progress in functional studies of transition metal borides," *Chinese Physics B,* vol. 30, no. 10, p. 108103, 2021.

[54] A. Sharma, V. Rangra, and A. Thakur, "Synthesis, properties, and applications of MBenes (two-dimensional metal borides) as emerging 2D materials: a review," *Journal of Materials Science,* pp. 1-14, 2022.

[55] H. Gunda *et al.*, "Progress, challenges, and opportunities in the synthesis, characterization, and application of metal-boride-derived two-dimensional nanostructures," *ACS Materials Letters,* vol. 3, no. 5, pp. 535-556, 2021.

[56] V. G. Nair, M. Birowska, D. Bury, M. Jakubczak, A. Rosenkranz, and A. M. Jastrzębska, "2D MBenes: A Novel Member in the Flatland," *Advanced Materials,* p. 2108840, 2022.

[57] S. K. John and A. A. Anappara, "Aqueous dispersions of highly luminescent boron-rich nanosheets by the exfoliation of polycrystalline titanium diboride," *New Journal of Chemistry,* vol. 43, no. 25, pp. 9953-9960, 2019.

[58] R. Patidar, H. Gunda, A. K. Varma, R. Gawas, S. K. Das, and K. Jasuja, "Co-solvent exfoliation of layered titanium diboride into few-layer-thick nanosheets," *Ceramics International,* vol. 46, no. 18, pp. 28324-28331, 2020.

[59] M. Yi and Z. Shen, "A review on mechanical exfoliation for the scalable production of graphene," *Journal of Materials Chemistry A,* vol. 3, no. 22, pp. 11700-11715, 2015.

[60] L. Niu, J. N. Coleman, H. Zhang, H. Shin, M. Chhowalla, and Z. Zheng, "Production of two-dimensional nanomaterials via liquid-based direct exfoliation," *Small,* vol. 12, no. 3, pp. 272-293, 2016.

[61] J. Yu, J. Li, W. Zhang, and H. Chang, "Synthesis of high quality two-dimensional materials via chemical vapor deposition," *Chemical science,* vol. 6, no. 12, pp. 6705-6716, 2015.

[62] M. Zeng, Y. Xiao, J. Liu, K. Yang, and L. Fu, "Exploring Two-Dimensional Materials toward the Next-Generation Circuits: From Monomer Design to Assembly Control," *Chem Rev,* vol. 118, no. 13, pp. 6236-6296, Jul 11 2018.

[63] M. Cai, D. Thorpe, D. H. Adamson, and H. C. Schniepp, "Methods of graphite exfoliation," *Journal of Materials Chemistry,* vol. 22, no. 48, pp. 24992-25002, 2012.

[64] A. Ciesielski and P. Samorì, "Graphene via sonication assisted liquid-phase exfoliation," *Chemical Society Reviews,* vol. 43, no. 1, pp. 381-398, 2014.

[65] S. H. Choi *et al.*, "Large-scale synthesis of graphene and other 2D materials towards industrialization," *Nature Communications,* vol. 13, no. 1, p. 1484, 2022.

[66] J. H. Warner, F. Schaffel, M. Rummeli, and A. Bachmatiuk, *Graphene: Fundamentals and emergent applications*. Newnes, 2012.

[67] W. Gao, *Graphene oxide: reduction recipes, spectroscopy, and applications*. Springer, 2015.

[68] S. Park and R. S. Ruoff, "Chemical methods for the production of graphenes," *Nature nanotechnology,* vol. 4, no. 4, pp. 217-224, 2009.

[69] E. Gao, S.-Z. Lin, Z. Qin, M. J. Buehler, X.-Q. Feng, and Z. Xu, "Mechanical exfoliation of two-dimensional materials," *Journal of the Mechanics and Physics of Solids,* vol. 115, pp. 248-262, 2018.

[70] W. Gao, "The chemistry of graphene oxide," *Graphene oxide: reduction recipes, spectroscopy, and applications,* pp. 61-95, 2015.

[71] Y. Xu, H. Cao, Y. Xue, B. Li, and W. Cai, "Liquid-phase exfoliation of graphene: an overview on exfoliation media, techniques, and challenges," *Nanomaterials,* vol. 8, no. 11, p. 942, 2018.

[72] K. R. Paton *et al.*, "Scalable production of large quantities of defect-free few-layer graphene by shear exfoliation in liquids," *Nature materials,* vol. 13, no. 6, pp. 624-630, 2014.

[73] J. M. Tour, "Scaling up exfoliation," *Nature materials,* vol. 13, no. 6, pp. 545-546, 2014.

[74] X. Gu *et al.*, "Method of ultrasound-assisted liquid-phase exfoliation to prepare graphene," *Ultrasonics Sonochemistry,* vol. 58, p. 104630, 2019.

[75] A. Mostovoy and A. Yakovlev, "Reinforcement of epoxy composites with graphite-graphene structures," *Scientific Reports,* vol. 9, no. 1, p. 16246, 2019.

[76] M. Yi, Z. Shen, S. Liang, L. Liu, X. Zhang, and S. Ma, "Water can stably disperse liquid-exfoliated graphene," *Chemical Communications,* vol. 49, no. 94, pp. 11059-11061, 2013.

[77]   T.-C. Wu *et al.*, "Inkjet-printed CMOS-integrated graphene–metal oxide sensors for breath analysis," *npj 2D Materials and Applications,* vol. 3, no. 1, p. 42, 2019.

[78]   L. Xu *et al.*, "Graphene-based biosensors for the detection of prostate cancer protein biomarkers: a review," *BMC chemistry,* vol. 13, pp. 1-12, 2019.

[79]   D. Selvakumar, H. Sivaram, A. Alsalme, A. Alghamdi, and R. Jayavel, "Freestanding flexible, pure and composite form of reduced graphene oxide paper for ammonia vapor sensing," *Scientific Reports,* vol. 9, no. 1, p. 8749, 2019.

[80]   N. Somani, Y. Tyagi, P. Kumar, V. Srivastava, and H. Bhowmick, "Enhanced tribological properties of SiC reinforced copper metal matrix composites," *Materials Research Express,* vol. 6, no. 1, p. 016549, 2018.

[81]   M. Lotya, P. J. King, U. Khan, S. De, and J. N. Coleman, "High-concentration, surfactant-stabilized graphene dispersions," *ACS nano,* vol. 4, no. 6, pp. 3155-3162, 2010.

[82]   L. A. Belyaeva, P. M. van Deursen, K. I. Barbetsea, and G. F. Schneider, "Hydrophilicity of graphene in water through transparency to polar and dispersive interactions," *Advanced materials,* vol. 30, no. 6, p. 1703274, 2018.

[83]   M. Buzaglo, M. Shtein, S. Kober, R. Lovrinčić, A. Vilan, and O. Regev, "Critical parameters in exfoliating graphite into graphene," *Physical Chemistry Chemical Physics,* vol. 15, no. 12, pp. 4428-4435, 2013.

[84]   L. Huang, Y. Huang, J. Liang, X. Wan, and Y. Chen, "Graphene-based conducting inks for direct inkjet printing of flexible conductive patterns and their applications in electric circuits and chemical sensors," *Nano Research,* vol. 4, pp. 675-684, 2011.

[85]   P. G. Karagiannidis *et al.*, "Microfluidization of graphite and formulation of graphene-based conductive inks," *ACS nano,* vol. 11, no. 3, pp. 2742-2755, 2017.

[86]   K. M. Shahil and A. A. Balandin, "Graphene–multilayer graphene nanocomposites as highly efficient thermal interface materials," *Nano letters,* vol. 12, no. 2, pp. 861-867, 2012.

[87]   A. S. Wajid *et al.*, "Polymer-stabilized graphene dispersions at high concentrations in organic solvents for composite production," *Carbon,* vol. 50, no. 2, pp. 526-534, 2012.

[88]   Z. Ismail, N. F. A. Kassim, A. H. Abdullah, A. S. Z. Abidin, F. S. Ismail, and K. Yusoh, "Black tea assisted exfoliation using a kitchen mixer allowing one-step production of graphene," *Materials Research Express,* vol. 4, no. 7, p. 075607, 2017.

[89]   V. Chabot, B. Kim, B. Sloper, C. Tzoganakis, and A. Yu, "High yield production and purification of few layer graphene by Gum Arabic assisted physical sonication," *Scientific reports,* vol. 3, no. 1, p. 1378, 2013.

[90]   P. Turner, M. Hodnett, R. Dorey, and J. D. Carey, "Controlled sonication as a route to in-situ graphene flake size control," *Scientific reports,* vol. 9, no. 1, p. 8710, 2019.

[91]   M. S. Gilliam *et al.*, "Evaluating the Exfoliation Efficiency of Quasi-2D Metal Diboride Nanosheets Using Hansen Solubility Parameters," *Langmuir,* vol. 37, no. 3, pp. 1194-1205, 2021.

[92]   X. Hu *et al.*, "Two-dimensional transition metal diborides: promising Dirac electrocatalysts with large reaction regions toward efficient N 2 fixation," *Journal of Materials Chemistry A,* vol. 7, no. 45, pp. 25887-25893, 2019.

[93]   S. Chakrabarty, A. Thakur, A. Rasyotra, B. Gaykwad, and K. Jasuja, "Quasi-two-dimensional nanostructures from AlB2-type metal borides: physicochemical insights and emerging trends," *The Journal of Physical Chemistry C,* vol. 127, no. 2, pp. 852-870, 2022.

[94]   J. Kim *et al.*, "Direct exfoliation and dispersion of two-dimensional materials in pure water via temperature control," *Nature communications,* vol. 6, no. 1, p. 8294, 2015.

[95]   S. Barwich, U. Khan, and J. N. Coleman, "A technique to pretreat graphite which allows the rapid dispersion of defect-free graphene in solvents at high concentration," *The Journal of Physical Chemistry C,* vol. 117, no. 37, pp. 19212-19218, 2013.

[96]   J.-H. Ding, H.-R. Zhao, and H.-B. Yu, "A water-based green approach to large-scale production of aqueous compatible graphene nanoplatelets," *Scientific Reports,* vol. 8, no. 1, p. 5567, 2018.

[97]   N. Zheng, L. Wang, and Z. Sun, "The effects of ultrasonication power and time on the dispersion stability of few-layer graphene nanofluids under the constant ultrasonic energy consumption condition," *Ultrasonics Sonochemistry,* vol. 80, p. 105816, 2021.

[98]   M. Bahiraei and S. Heshmatian, "Graphene family nanofluids: A critical review and future research directions," *Energy Conversion and Management,* vol. 196, pp. 1222-1256, 2019.

[99]   A. Afzal, I. Nawfal, I. Mahbubul, and S. S. Kumbar, "An overview on the effect of ultrasonication duration on different properties of nanofluids," *Journal of Thermal Analysis and Calorimetry,* vol. 135, no. 1, pp. 393-418, 2019.

[100] I. Mahbubul, E. B. Elcioglu, R. Saidur, and M. Amalina, "Optimization of ultrasonication period for better dispersion and stability of TiO2–water nanofluid," *Ultrasonics sonochemistry,* vol. 37, pp. 360-367, 2017.

[101] J. H. Bang and K. S. Suslick, "Applications of ultrasound to the synthesis of nanostructured materials," *Advanced materials,* vol. 22, no. 10, pp. 1039-1059, 2010.

[102] H. Zhu, C. Li, D. Wu, C. Zhang, and Y. Yin, "Preparation, characterization, viscosity and thermal conductivity of CaCO 3 aqueous nanofluids," *Science China Technological Sciences,* vol. 53, pp. 360-368, 2010.

[103] P. Wolski, "Sonification energy in the process of ultrasonic disintegration," *Journal of Ecological Engineering,* vol. 21, no. 3, pp. 36-40, 2020.

[104] A. V. Tyurnina *et al.*, "Ultrasonic exfoliation of graphene in water: A key parameter study," *Carbon,* vol. 168, pp. 737-747, 2020.

[105] X. Xiao, H. Wang, P. Urbankowski, and Y. Gogotsi, "Topochemical synthesis of 2D materials," *Chem Soc Rev,* vol. 47, no. 23, pp. 8744-8765, Nov 26 2018.

[106] T. H. Le, Y. Oh, H. Kim, and H. Yoon, "Exfoliation of 2D Materials for Energy and Environmental Applications," *Chemistry,* vol. 26, no. 29, pp. 6360-6401, May 20 2020.

[107] A. K. Geim and K. S. Novoselov, "The rise of graphene," in *Nanoscience and technology: a collection of reviews from nature journals*: World Scientific, 2010, pp. 11-19.

[108] N. Ortiz and S. E. Skrabalak, "On the dual roles of ligands in the synthesis of colloidal metal nanostructures," *Langmuir,* vol. 30, no. 23, pp. 6649-6659, 2014.

[109] S. Yang, P. Qiu, and G. Yang, "Graphene induced formation of single crystal Pt nanosheets through 2-dimensional aggregation and sintering of nanoparticles in molten salt medium," *Carbon,* vol. 77, pp. 1123-1131, 2014.

[110] S. E. Skrabalak, B. J. Wiley, M. Kim, E. V. Formo, and Y. Xia, "On the polyol synthesis of silver nanostructures: glycolaldehyde as a reducing agent," *Nano letters,* vol. 8, no. 7, pp. 2077-2081, 2008.

[111] H. Samassekou *et al.*, "Viable route towards large-area 2D MoS2 using magnetron sputtering," *2D Materials,* vol. 4, no. 2, p. 021002, 2017.

[112] W. Yu *et al.*, "Flexible 2D materials beyond graphene: synthesis, properties, and applications," *Small,* vol. 18, no. 14, p. 2105383, 2022.

[113] R. Raccichini, A. Varzi, S. Passerini, and B. Scrosati, "The role of graphene for electrochemical energy storage," *Nature materials,* vol. 14, no. 3, pp. 271-279, 2015.

[114] K. S. Novoselov, V. I. Fal′ ko, L. Colombo, P. R. Gellert, M. G. Schwab, and K. Kim, "A roadmap for graphene," *nature,* vol. 490, no. 7419, pp. 192-200, 2012.

[115] S. Alam, M. A. Chowdhury, A. Shahid, R. Alam, and A. Rahim, "Synthesis of emerging two-dimensional (2D) materials–Advances, challenges and prospects," *FlatChem,* vol. 30, p. 100305, 2021.

[116] C. An *et al.*, "Ultrasonic-assisted preparation of two-dimensional materials for electrocatalysts," *Ultrasonics Sonochemistry,* p. 106503, 2023.

[117] J. Zhan, Z. Zhang, X. Qian, C. Wang, Y. Xie, and Y. Qian, "Solvothermal Synthesis of Nanocrystalline MoS2from MoO3and Elemental Sulfur," *Journal of Solid State Chemistry,* vol. 141, no. 1, pp. 270-273, 1998.

[118] L. Yang, W. Chen, Q. Yu, and B. Liu, "Mass production of two-dimensional materials beyond graphene and their applications," *Nano Research,* vol. 14, pp. 1583-1597, 2021.

[119] F. Torrisi *et al.*, "Inkjet-printed graphene electronics," *ACS nano,* vol. 6, no. 4, pp. 2992-3006, 2012.

[120] J. Li, F. Ye, S. Vaziri, M. Muhammed, M. C. Lemme, and M. Östling, "Efficient inkjet printing of graphene," *Advanced materials,* vol. 25, no. 29, pp. 3985-3992, 2013.

[121] H. Gu, H. Tang, P. Xiong, and Z. Zhou, "Biomarkers-based biosensing and bioimaging with graphene for cancer diagnosis," *Nanomaterials,* vol. 9, no. 1, p. 130, 2019.

[122] J. Abraham *et al.*, "Tunable sieving of ions using graphene oxide membranes," *Nature nanotechnology,* vol. 12, no. 6, pp. 546-550, 2017.

[123] W. Kong *et al.*, "Path towards graphene commercialization from lab to market," *Nature nanotechnology,* vol. 14, no. 10, pp. 927-938, 2019.

[124] G. Chen *et al.*, "Preparation and characterization of graphite nanosheets from ultrasonic powdering technique," *Carbon,* vol. 42, no. 4, pp. 753-759, 2004.

[125] S. Stankovich, R. D. Piner, S. T. Nguyen, and R. S. Ruoff, "Synthesis and exfoliation of isocyanate-treated graphene oxide nanoplatelets," *Carbon,* vol. 44, no. 15, pp. 3342-3347, 2006.

[126] M. Jin *et al.*, "Facile physical route to highly crystalline graphene," *Advanced Functional Materials,* vol. 21, no. 18, pp. 3496-3501, 2011.

[127]   J. Wan, S. D. Lacey, J. Dai, W. Bao, M. S. Fuhrer, and L. Hu, "Tuning two-dimensional nanomaterials by intercalation: materials, properties and applications," *Chemical Society Reviews,* vol. 45, no. 24, pp. 6742-6765, 2016.

[128]   J. N. Coleman *et al.*, "Two-dimensional nanosheets produced by liquid exfoliation of layered materials," *Science,* vol. 331, no. 6017, pp. 568-571, 2011.

[129]   C. Mellado, T. Figueroa, R. Baez, M. Meléndrez, and K. Fernández, "Effects of probe and bath ultrasonic treatments on graphene oxide structure," *Materials Today Chemistry,* vol. 13, pp. 1-7, 2019.

[130]   A. Liscio *et al.*, "Evolution of the size and shape of 2D nanosheets during ultrasonic fragmentation," *2D Materials,* vol. 4, no. 2, p. 025017, 2017.

[131]   A. Amiri, M. Naraghi, G. Ahmadi, M. Soleymaniha, and M. Shanbedi, "A review on liquid-phase exfoliation for scalable production of pure graphene, wrinkled, crumpled and functionalized graphene and challenges," *FlatChem,* vol. 8, pp. 40-71, 2018.

[132]   S. Meng, T. Kong, W. Ma, H. Wang, and H. Zhang, "2D crystal–based fibers: Status and challenges," *Small,* vol. 15, no. 39, p. 1902691, 2019.

[133]   H. Juretschke and R. Steinitz, "Hall effect and electrical conductivity of transition-metal diborides," *Journal of Physics and Chemistry of Solids,* vol. 4, no. 1-2, pp. 118-127, 1958.

[134]   X.-B. Wang, D.-C. Tian, and L.-L. Wang, "The electronic structure and chemical stability of the AlB2-type transition-metal diborides," *Journal of Physics: Condensed Matter,* vol. 6, no. 46, p. 10185, 1994.

[135]   M. Schneider *et al.*, "Heat and charge transport properties of MgB2," *Physica C: Superconductivity,* vol. 363, no. 1, pp. 6-12, 2001.

[136]   C. Buzea and T. Yamashita, "Review of the superconducting properties of MgB2," *Superconductor Science and Technology,* vol. 14, no. 11, p. R115, 2001.

[137]   H. Ihara, M. Hirabayashi, and H. Nakagawa, "Band structure and x-ray photoelectron spectrum of Zr B 2," *Physical Review B,* vol. 16, no. 2, p. 726, 1977.

[138]   B. Mouffok, H. Feraoun, and H. Aourag, "Electronic structure of some mono-, semi-titanium boride and diboride," *Materials Letters,* vol. 60, no. 12, pp. 1433-1436, 2006.

[139]   P. Perkins and A. Sweeney, "An investigation of the electronic band structures of NaB6, KB6, TiB2, and CrB," *Journal of the Less Common Metals,* vol. 47, pp. 165-173, 1976.

[140] K. E. Spear, "Chemical bonding in AlB2-type borides," *Journal of the Less Common Metals,* vol. 47, pp. 195-201, 1976.

[141] F. R. Wagner, A. I. Baranov, Y. Grin, and M. Kohout, "A Position-Space View on Chemical Bonding in Metal Diborides with AlB2 Type of Crystal Structure," *Zeitschrift für anorganische und allgemeine Chemie,* vol. 639, no. 11, pp. 2025-2035, 2013.

[142] I. R. Shein and A. L. Ivanovskii, "Elastic properties of mono-and polycrystalline hexagonal AlB2-like diborides of s, p and d metals from first-principles calculations," *Journal of Physics: Condensed Matter,* vol. 20, no. 41, p. 415218, 2008.

[143] S. Haar *et al.*, "Enhancing the liquid-phase exfoliation of graphene in organic solvents upon addition of n-octylbenzene," *Scientific reports,* vol. 5, no. 1, p. 16684, 2015.

[144] E. P. Nguyen *et al.*, "Investigation of two-solvent grinding-assisted liquid phase exfoliation of layered MoS2," *Chemistry of Materials,* vol. 27, no. 1, pp. 53-59, 2015.

[145] R. Boucher, "Sonochemistry at low and high ultrasonic frequencies," *British Chemical Engineering,* vol. 15, no. 3, pp. 363-&, 1970.

[146] G. Bepete *et al.*, "Surfactant-free single-layer graphene in water," *Nature Chemistry,* vol. 9, no. 4, pp. 347-352, 2017.

[147] M. Tan, N. Chin, Y. Yusof, F. Taip, and J. Abdullah, "Characterisation of improved foam aeration and rheological properties of ultrasonically treated whey protein suspension," *International Dairy Journal,* vol. 43, pp. 7-14, 2015.

[148] M. Abd Mutalib, M. Rahman, M. Othman, A. Ismail, and J. Jaafar, "Scanning electron microscopy (SEM) and energy-dispersive X-ray (EDX) spectroscopy," in *Membrane characterization*: Elsevier, 2017, pp. 161-179.

[149] J. Liu and J. Cowley, "High-resolution scanning transmission electron microscopy," *Ultramicroscopy,* vol. 52, no. 3-4, pp. 335-346, 1993.

[150] Cirp, *CIRP Encyclopedia of Production Engineering*. 2014.

[151] J. P. Painuly, "Barriers to renewable energy penetration; a framework for analysis," *Renewable energy,* vol. 24, no. 1, pp. 73-89, 2001.

[152] F. J. Giessibl, "Advances in atomic force microscopy," *Reviews of modern physics,* vol. 75, no. 3, p. 949, 2003.

[153] I. Musevic, "Atomic force microscopy," *INFORMACIJE MIDEM-LJUBLJANA-,* no. 4, pp. 223-227, 2000.

[154]   A. Imberg, H. Evertsson, P. Stilbs, M. Kriechbaum, and S. Engström, "On the self-assembly of monoolein in mixtures of water and a polar aprotic solvent," *The Journal of Physical Chemistry B,* vol. 107, no. 10, pp. 2311-2318, 2003.

[155]   J. Wu, J. Wang, X. Huang, and H. Bai, "A self-assembly route to porous polyaniline/reduced graphene oxide composite materials with molecular-level uniformity for high-performance supercapacitors," *Energy & Environmental Science,* vol. 11, no. 5, pp. 1280-1286, 2018.

[156]   W. Zhao *et al.*, "Direct exfoliation of natural SiO2-containing molybdenite in isopropanol: a cost efficient solution for large-scale production of MoS2 nanosheetes," *Nanomaterials,* vol. 8, no. 10, p. 843, 2018.

[157]   Y. Wang *et al.*, "Intercalated 2D MoS2 utilizing a simulated sun assisted process: reducing the HER overpotential," *The Journal of Physical Chemistry C,* vol. 120, no. 4, pp. 2447-2455, 2016.

[158]   J. Wu *et al.*, "Exfoliated 2D transition metal disulfides for enhanced electrocatalysis of oxygen evolution reaction in acidic medium," *Advanced Materials Interfaces,* vol. 3, no. 9, p. 1500669, 2016.

[159]   G. Lv, J. Wang, Z. Shi, and L. Fan, "Intercalation and delamination of two-dimensional MXene (Ti3C2Tx) and application in sodium-ion batteries," *Materials Letters,* vol. 219, pp. 45-50, 2018.

[160]   J. Wu *et al.*, "Highly safe and ionothermal synthesis of Ti3C2 MXene with expanded interlayer spacing for enhanced lithium storage," *Journal of Energy Chemistry,* vol. 47, pp. 203-209, 2020.

[161]   S. M. Beladi-Mousavi, A. M. Pourrahimi, Z. Sofer, and M. Pumera, "Atomically thin 2D-arsenene by liquid-phased exfoliation: toward selective vapor sensing," *Advanced Functional Materials,* vol. 29, no. 5, p. 1807004, 2019.

[162]   J. Zheng *et al.*, "High yield exfoliation of two-dimensional chalcogenides using sodium naphthalenide," *Nature communications,* vol. 5, no. 1, p. 2995, 2014.

[163]   C. F. Holder and R. E. Schaak, "Tutorial on powder X-ray diffraction for characterizing nanoscale materials," vol. 13, ed: ACS Publications, 2019, pp. 7359-7365.

[164]   K. Nakagawa *et al.*, "Enhanced photocatalytic hydrogen evolution from water by niobate single molecular sheets and ensembles," *Chemical Communications,* vol. 50, no. 89, pp. 13702-13705, 2014.

[165]   A. Shmeliov *et al.*, "Impurity induced non-bulk stacking in chemically exfoliated h-BN nanosheets," *Nanoscale,* vol. 5, no. 6, pp. 2290-2294, 2013.

[166] A. Ambrosi and M. Pumera, "Electrochemically exfoliated graphene and graphene oxide for energy storage and electrochemistry applications," *Chemistry–A European Journal,* vol. 22, no. 1, pp. 153-159, 2016.

[167] T. Skaltsas, N. Karousis, H.-J. Yan, C.-R. Wang, S. Pispas, and N. Tagmatarchis, "Graphene exfoliation in organic solvents and switching solubility in aqueous media with the aid of amphiphilic block copolymers," *Journal of Materials Chemistry,* vol. 22, no. 40, pp. 21507-21512, 2012.

[168] Y. Xue, Q. Zhang, W. Wang, H. Cao, Q. Yang, and L. Fu, "Opening two-dimensional materials for energy conversion and storage: A concept," *Advanced Energy Materials,* vol. 7, no. 19, p. 1602684, 2017.

[169] L. Yang *et al.*, "Enhanced photocatalytic activity of g-C3N4 2D nanosheets through thermal exfoliation using dicyandiamide as precursor," *Ceramics International,* vol. 44, no. 17, pp. 20613-20619, 2018.

[170] W. Zhang *et al.*, "Soluble, exfoliated two-dimensional nanosheets as excellent aqueous lubricants," *ACS Applied Materials & Interfaces,* vol. 8, no. 47, pp. 32440-32449, 2016.

[171] Z. Li *et al.*, "N-methyl-2-pyrrolidone Iodide as Functional Precursor Additive for Record Efficiency 2D Ruddlesden-Popper (PEA) 2 (Cs) n− 1PbnI3n+ 1 Solar Cells," *Advanced Functional Materials,* vol. 31, no. 52, p. 2106380, 2021.

[172] J. Fan, Z. Shi, L. Zhang, J. Wang, and J. Yin, "Aramid nanofiber-functionalized graphene nanosheets for polymer reinforcement," *Nanoscale,* vol. 4, no. 22, pp. 7046-7055, 2012.

[173] M. U. Arshad, H. Raza, M. B. Khan, and A. Hussain, "Synthesis of 2D Molybdenum Disulfide (MoS2) for enhancement of mechanical and electrical properties of polystyrene (PS) polymer," *Polymer Testing,* vol. 90, p. 106646, 2020.

[174] P. M. Pataniya *et al.*, "Flexible paper based piezo-resistive sensor functionalised by 2D-WSe2 nanosheets," *Nanotechnology,* vol. 31, no. 43, p. 435503, 2020.

[175] M. Liang *et al.*, "Improving stability of organometallic-halide perovskite solar cells using exfoliation two-dimensional molybdenum chalcogenides," *npj 2D Materials and Applications,* vol. 4, no. 1, p. 40, 2020.

[176] V. Guerra and T. McNally, "Surface cleaning of 2D materials: boron nitride nanosheets (BNNS) and exfoliated graphite nanoplatelets (GNP)," *Advanced Materials Interfaces,* vol. 7, no. 19, p. 2000944, 2020.

[177] A. Bianco *et al.*, "All in the graphene family–A recommended nomenclature for two-dimensional carbon materials," vol. 65, ed: Elsevier, 2013, pp. 1-6.

[178] W. Fu, H. Liu, X. Shi, L. Zuo, X. Li, and A. K. Y. Jen, "Tailoring the functionality of organic spacer cations for efficient and stable quasi-2D perovskite solar cells," *Advanced Functional Materials,* vol. 29, no. 25, p. 1900221, 2019.

[179] T. Taniguchi *et al.*, "Revisiting the two-dimensional structure and reduction process of graphene oxide with in-plane X-ray diffraction," *Carbon,* vol. 202, pp. 26-35, 2023.

[180] J. Shang, F. Xue, and E. Ding, "Efficient exfoliation of molybdenum disulphide nanosheets by a high-pressure homogeniser," *Micro & Nano Letters,* vol. 10, no. 10, pp. 589-591, 2015.

[181] G.-Q. Han *et al.*, "WS2 nanosheets based on liquid exfoliation as effective electrocatalysts for hydrogen evolution reaction," *Materials Chemistry and Physics,* vol. 167, pp. 271-277, 2015.

[182] D. Deepak *et al.*, "Surfactant gel-based method: A universal soft method for the exfoliation of 2D materials," *Journal of Colloid and Interface Science,* vol. 645, pp. 906-917, 2023.

[183] H. Shalchian *et al.*, "On the mechanism of molybdenite exfoliation during mechanical milling," *Ceramics International,* vol. 43, no. 15, pp. 12957-12967, 2017.

[184] M. Q. Zhao, N. Trainor, C. E. Ren, M. Torelli, B. Anasori, and Y. Gogotsi, "Scalable manufacturing of large and flexible sheets of MXene/graphene heterostructures," *Advanced Materials Technologies,* vol. 4, no. 5, p. 1800639, 2019.

[185] K. Muthoosamy and S. Manickam, "State of the art and recent advances in the ultrasound-assisted synthesis, exfoliation and functionalization of graphene derivatives," *Ultrasonics sonochemistry,* vol. 39, pp. 478-493, 2017.

[186] R. Jalili *et al.*, "Processable 2D materials beyond graphene: MoS 2 liquid crystals and fibres," *Nanoscale,* vol. 8, no. 38, pp. 16862-16867, 2016.

[187] Z. Wu *et al.*, "Novel sub-5 nm layered niobium phosphate nanosheets for high-voltage, cation-intercalation typed electrochemical energy storage in wearable pseudocapacitors," *Advanced Energy Materials,* vol. 9, no. 20, p. 1900111, 2019.

[188] V. Kaganer, R. Köhler, M. Schmidbauer, R. Opitz, and B. Jenichen, "X-ray diffraction peaks due to misfit dislocations in heteroepitaxial structures," *Physical Review B,* vol. 55, no. 3, p. 1793, 1997.

[189] Y. Jiang, L. Cao, X. Hu, Z. Ren, C. Zhang, and C. Wang, "Simulating powder X-ray diffraction patterns of two-dimensional materials," *Inorganic Chemistry,* vol. 57, no. 24, pp. 15123-15132, 2018.

[190]   S. Pilli, P. Bhunia, S. Yan, R. LeBlanc, R. Tyagi, and R. Surampalli, "Ultrasonic pretreatment of sludge: a review," *Ultrasonics sonochemistry,* vol. 18, no. 1, pp. 1-18, 2011.

[191]   I. Tzanakis, D. Eskin, A. Georgoulas, and D. Fytanidis, "Incubation pit analysis and calculation of the hydrodynamic impact pressure from the implosion of an acoustic cavitation bubble," *Ultrasonics Sonochemistry,* vol. 21, no. 2, pp. 866-878, 2014.

[192]   Y. Wang *et al.*, "Experimental and numerical investigation of cavitation-induced erosion in thermal sprayed single splats," *Ultrasonics Sonochemistry,* vol. 52, pp. 336-343, 2019.

[193]   Z. Shen, J. Li, M. Yi, X. Zhang, and S. Ma, "Preparation of graphene by jet cavitation," *Nanotechnology,* vol. 22, no. 36, p. 365306, 2011.

[194]   E. B. Flint and K. S. Suslick, "The temperature of cavitation," *Science,* vol. 253, no. 5026, pp. 1397-1399, 1991.

[195]   J. T. Han *et al.*, "Extremely efficient liquid exfoliation and dispersion of layered materials by unusual acoustic cavitation," *Scientific Reports,* vol. 4, no. 1, p. 5133, 2014.

[196]   I. Tzanakis, G. S. Lebon, D. Eskin, and K. A. Pericleous, "Characterisation of the ultrasonic acoustic spectrum and pressure field in aluminium melt with an advanced cavitometer," *Journal of Materials Processing Technology,* vol. 229, pp. 582-586, 2016.

[197]   T. Leighton, *The acoustic bubble*. Academic press, 2012.

[198]   L. Wang, G. Memoli, M. Hodnett, I. Butterworth, D. Sarno, and B. Zeqiri, "Towards a reference cavitating vessel Part III—design and acoustic pressure characterization of a multi-frequency sonoreactor," *Metrologia,* vol. 52, no. 4, p. 575, 2015.

[199]   S. Brems *et al.*, "Nanoparticle removal with megasonics: a review," *ECS Journal of Solid State Science and Technology,* vol. 3, no. 1, p. N3010, 2013.

[200]   M. Telkhozhayeva *et al.*, "Higher ultrasonic frequency liquid phase exfoliation leads to larger and monolayer to few-layer flakes of 2D layered materials," *Langmuir,* vol. 37, no. 15, pp. 4504-4514, 2021.

[201]   G. B. Lebon, I. Tzanakis, K. Pericleous, D. Eskin, and P. S. Grant, "Ultrasonic liquid metal processing: The essential role of cavitation bubbles in controlling acoustic streaming," *Ultrasonics sonochemistry,* vol. 55, pp. 243-255, 2019.

[202]   E. M. Joyce, X. Wu, and T. J. Mason, "Effect of ultrasonic frequency and power on algae suspensions," *Journal of Environmental Science and Health Part A,* vol. 45, no. 7, pp. 863-866, 2010.

[203] A. Kordylla, S. Koch, F. Tumakaka, and G. Schembecker, "Towards an optimized crystallization with ultrasound: Effect of solvent properties and ultrasonic process parameters," *Journal of Crystal Growth,* vol. 310, no. 18, pp. 4177-4184, 2008.

[204] M. Minnaert, "XVI. On musical air-bubbles and the sounds of running water," *The London, Edinburgh, and Dublin Philosophical Magazine and Journal of Science,* vol. 16, no. 104, pp. 235-248, 1933.

[205] I. Tzanakis, K. Pericleous, and D. Eskin, "Experimental and numerical investigation of acoustic pressures in different liquids," 2018.

[206] I. Tzanakis, G. Lebon, D. Eskin, and K. Pericleous, "Characterizing the cavitation development and acoustic spectrum in various liquids," *Ultrasonics sonochemistry,* vol. 34, pp. 651-662, 2017.

[207] C. Ohl and R. Ikink, "Shock-wave-induced jetting of micron-size bubbles," *Physical review letters,* vol. 90, no. 21, p. 214502, 2003.

[208] M. Sirotyuk, "Experimental investigations of ultrasonic cavitation," in *High-intensity ultrasonic fields*: Springer, 1971, pp. 261-343.

[209] L. Rozenberg, *High-intensity ultrasonic fields*. Springer Science & Business Media, 2013.

[210] K. Yasuda, H. Matsushima, and Y. Asakura, "Generation and reduction of bulk nanobubbles by ultrasonic irradiation," *Chemical Engineering Science,* vol. 195, pp. 455-461, 2019.

[211] T.-H. Kim and H.-Y. Kim, "Disruptive bubble behaviour leading to microstructure damage in an ultrasonic field," *Journal of fluid mechanics,* vol. 750, pp. 355-371, 2014.

[212] Q. Zeng, S. R. Gonzalez-Avila, R. Dijkink, P. Koukouvinis, M. Gavaises, and C.-D. Ohl, "Wall shear stress from jetting cavitation bubbles," *Journal of Fluid Mechanics,* vol. 846, pp. 341-355, 2018.

[213] J. A. Morton *et al.*, "New insights into sono-exfoliation mechanisms of graphite: In situ high-speed imaging studies and acoustic measurements," *Materials Today,* vol. 49, pp. 10-22, 2021.

[214] C. Petrier *et al.*, "Sonochemical degradation of phenol in dilute aqueous solutions: comparison of the reaction rates at 20 and 487 kHz," *The Journal of Physical Chemistry,* vol. 98, no. 41, pp. 10514-10520, 1994.